Technical University of Liberec
Faculty of Sciences, Humanities and Education
Department of Physics
Studentska 2, 461 17 Liberec 1, Czech Republic

www.tul.cz

Characterization of Piezoelectric Materials by Ultrasonic Technique

Dissertation

Liberec 2008 Volodymyr Ryzhenko

Technical University of Liberec
Faculty of Sciences, Humanities and Education
Department of Physics
Studentska 2, 461 17 Liberec 1, Czech Republic

www.tul.cz

Characterization of Piezoelectric Materials by Ultrasonic Technique

Dissertation

Graduant: Volodymyr Ryzhenko
Dissertation Supervisor: Doc. Mgr. Lidmila Burianova, CSc.
Consultant: Doc. RNDr. Antonin Kopal, CSc.
Workplace: Department of Physics, Piezoelectric Laboratory
Study programme: Applied Sciences in Engineering
Branch of Study: Physical Engineering

Number of pages: 68
Number of figures: 52
Number of tables: 1
Number of equations: 24

Place and year: *Liberec 2008*

…… ……
Place and date *Author*'s *signature*

Prohlášení

Byl jsem seznámen s tím, že na mou disertační práci se plně vztahuje zákon č. 121/2000 Sb. o právu autorském, zejména § 60 – školní dílo.

Beru na vědomí, že Technická univerzita v Liberci (TUL) nezasahuje do mých autorských práv užitím mé disertační práce pro vnitřní potřebu TUL.

Užiji-li disertační práci nebo poskytnu-li licenci k jejímu využití, jsem si vědom povinnosti informovat o této skutečnosti TUL; v tomto případě má TUL právo ode mne požadovat úhradu nákladů, které vynaložila na vytvoření díla, až do jejich skutečné výše.

Disertační práci jsem vypracoval samostatně s použitím uvedené literatury a na základě konzultací s vedoucím disertační práce a konzultantem.

V Liberci dne: 15.8.2008 Volodymyr Ryzhenko

.....

Acknowledgements

I would like to thank my dissertation supervisor Lidmila Burianová for her help, valuable advice and encouragement during my postgraduate studies. I must also express my thanks to Antonín Kopal for language corrections, and Petr Hána for his advice during the experiment preparation.

Materiálová charakterizace piezoelektrických látek s využitím ultrazvukové metody

Anotace

Disertační práce je zaměřena na materiálovou charakterizaci vybraných piezoelektrických látek ($Pb(Zr_xTi_{1-x})O_3$ (PZT) keramiky a $Pb(Zr_{1/3}Nb_{2/3})O_3$-$PbTiO_3$ (PZN-PT) krystalů) s využitím ultrazvukové metody. Experimentálně jsou určeny rychlosti šíření ultrazvuku v podélném a příčném směru, stanoven útlum a vypočteny elastické koeficienty PZT keramiku s předpokládanou symetrií ∞mm. Byly měřeny vzorky piezoelektrické keramiky PZT definovaných tvarů a rozměrů, jako je kruhová destička, tyčinka a pravoúhlá tenká destička. Součástí práce je také návrh speciálního držáku pro měření v elektrickém poli při experimentálním studiu nelineárních jevů, jako je vliv stejnosměrného elektrického pole na rychlosti šíření ultrazvuku. Hledal se optimální způsob měření vzorků v teplotní komůrce. Vyvinutý program řídí ultrazvuková měření a automaticky vyhodnocuje získaná data.

Diskutovány jsou možnosti ultrazvukové metody, její výhody a nevýhody. Jsou navrženy tvary vzorků, umožňující zvýšení přesnosti měření. Zvláštní pozornost je věnována oblasti fázových přechodů feroelektrických materiálů. Práce se proto zabývá studiem teplotní závislosti rychlosti šíření ultrazvuku a jeho útlumu při fázových přechodech ve feroelektrických materiálech. Byla pozorována změna teplotní závislosti rychlosti šíření na teplotě pro různé feroelektrické fáze. Fázové přechody jsou indikovány extrémy v teplotní závislosti rychlosti ultrazvukové vlny.

Klíčová slova: PZT keramika, PZN-PT krystaly, podélná a příčna vlna, ultrazvuková fázová rychlost a útlum, strukturní fázový přechod.

Characterization of Piezoelectric Materials by Ultrasonic Technique

Summary

The thesis deals with the material characterization of some piezoelectric materials, like $Pb(Zr_xTi_{1-x})O_3$ (PZT) ceramics and $Pb(Zr_{1/3}Nb_{2/3})O_3$-$PbTiO_3$ (PZN-PT) crystals by ultrasonic method. The velocities of propagation of ultrasound polarized in longitudinal and transverse direction were determined experimentally. The elastic coefficients of PZT ceramics with supposed symmetry ∞mm were determined, the attenuation was calculated. The measurement proceeded on piezoelectric ceramics PZT samples of defined forms and proportions: circular plate, bar and rectangular plate. For experimental study of the nonlinear effects, like the influence of bias electric field on velocity of ultrasound wave propagation, a special sample holder was designed. The optimal method for the measurement under electric field in thermal chamber was developed. The method for data processing of ultrasonic measurements was proposed in order to perform an automated measurement.

The possibilities, benefits and disadvantages of the ultrasonic methods are discussed. Samples shapes, which enable to increase an accuracy of measurement, were designed. Special attention was focused on the temperature regions of phase transitions in investigated materials. The work also deals with temperature dependence of velocity and attenuation of ultrasound propagation during phase transition in ferroelectric materials. The changes in dependence of velocity of ultrasound propagation on temperature for various ferroelectric phases were observed. Phase transitions were indicated by extremes in temperature dependence of ultrasonic waves velocity.

Keywords: PZT ceramics, PZN-PT single crystal, longitudinal and shear waves, ultrasonic phase velocity and attenuation, structural phase transition.

Характеризация свойств пьезоэлектрических материалов при помощи ультразвукового метода

Абстракт

Диссертация направлена на характеризацию свойств некоторых пьезоэлектрических материалов, как $Pb(Zr_xTi_{1-x})O_3$ (PZT) керамика и $Pb(Zr_{1/3}Nb_{2/3})O_3$-$PbTiO_3$ (PZN-PT) кристаллы, при помощи ультразвукового метода. Экспериментально были определены скорости распространения ультразвуковых волн, поляризованных в продольном и поперечном направлении. Были определены некоторые коэффициенты эластичности керамики PZT с предполагаемой симметрией ∞mm, а также были вычислены коэффициенты ослабления ультразвука. Измерения производились на образцах пьезоэлектрической керамики PZT определенных форм и пропорций: круглые пластины, палочки и прямоугольные пластины. Для экспериментального исследования нелинейных эффектов, таких как влияние электрического поля на скорость распространения ультразвуковых волн, был разработан специальный держатель образцов. Также был разработан оптимальный метод измерения под влиянием электрического поля в температурной камере и предложен метод для автоматического управления и обработки данных ультразвуковых измерений. Обсуждены возможности, преимущества и недостатки методов измерений ультразвуком. Для улучшения точности измерений были выбраны наиболее пригодные формы образцов. При исследовании материалов особое внимание было сосредоточено на область температур фазовых переходов. Работа также имеет дело с температурной зависимостью скорости распространения и ослабления ультразвука в области фазовых переходов в сегнетоэлектрических материалах. Для различных сегнетоэлектрических фаз наблюдались изменения в зависимости скорости распространения ультразвука от температуры. Фазовые переходы были обнаружены в виде экстремумов в температурной зависимости скорости ультразвуковых волн.

Ключевые слова: PZT керамика, PZN-PT кристаллы, продольная и поперечная волна, ультразвуковая фазовая скорость и затухание, структурный фазовый переход.

TABLE OF CONTENTS

List of symbols:

A_i	magnitude of i-th echo response
$\vec{B}$	the vector of the magnetic field
c^E_{ijkl}	components of the tensor of elastic moduli
$\vec{D}$	displacement vector
D_i	displacement vector components
d_{ijk}, $d_{i\lambda}$	piezoelectric coefficients
d	thickness of the sample
e_{kij}	piezoelectric constants
$\vec{E}$	the vector of the electric field intensity
E_j	the vector component of the electric field intensity
E_c	coercive electric field
k_{33}	the electromechanical coupling coefficient
l	width of the sample
$\vec{P}$	vector of polarization
S_{kl}	the strain tensor
T_{ij}	the stress tensor
T	temperature
T_c	Curie temperature
t	time
V	sound velocity
v_i	vector component of polarization of plane wave in a given direction
α	attenuation coefficient
ε_{ij}	the dielectric permittivity tensor
ε^T_{11}, ε^T_{33}	components of the tensor of dielectric permittivity at constant stress T

ε_{11}^{S}, ε_{33}^{S}	components of the tensor of dielectric permittivity at constant strain S
ρ	material density
$\delta\tau$, τ	time of flight between two ultrasound echoes
u_{i}	vector component of mechanical displacement
Γ_{il}	Christoffel tensor for unpiezoelectric material
$\bar{\Gamma}_{\mathrm{il}}$	Christoffel tensor for piezoelectric material
Φ_0	amplitude of the electric potential
Φ	electric potential
$v_{\mathrm{shear}[010]}^{[100]}$	the velocity of propagation of shear ultrasound waves in [100] direction, polarized in [010] direction
$v_{\mathrm{long}}^{[100]}$	the velocity of propagation of longitudinal ultrasound waves in [100] direction

1. Introduction

1.1 Overview

Ultrasound is a vibration that travels through an elastic medium as a wave on frequencies higher then frequency limit of audibility of the human ear, i.e. 20 kHz. The speed of ultrasound describes how much distance such a wave travels in a certain amount of time. For diagnostic purposes however employs high frequency in megahertz areas. The ultrasonic oscillations of elastic environment expands through the sample in the form of longitudinal or shear waves. In a non-dispersive medium sound speed is independent of sound frequency, so the speeds of energy transport and sound propagation are the same. In a dispersive medium sound speed is a function of sound frequency. The spatial and temporal distribution of a propagating disturbance will continually change. Each frequency component propagates at its own phase velocity, while the energy of the disturbance propagates at the group velocity. The speed of sound is variable and depends mainly on the temperature and the properties of the substance through of which the wave is traveling. We supposed that in our measurements the phase velocity is approximately the same as a group velocity. The source of ultrasonic oscillations for diagnostic purposes are mainly electrically excited piezoelectric transducers. Every environment is from acoustical aspects characterized by several characteristics. Most important of them are the velocity of propagation of ultrasound wave through given environment (so - called phase velocity), acoustic impedance and attenuation. The quantity of acoustic energy reflected on acoustic interface, is a function of the difference of materials acoustic impedance, forming this interface. The elastic features of the material and the characterization of domain structures of ferroelectric materials can be made from the measurements of speed and attenuation of ultrasound waves. The knowledge of material parameters, i. e. elastic, piezoelectric and dielectric constants of anisotropic environment is important for application of piezoelectric materials in the area of sensors, actuators, converters or piezoelectric resonators.

Lead zirconate titanate (PZT) ceramics are commercially the most important piezoelectric materials because of their adjustable properties, and the ability to tailoring their properties, either by changing the composition or by doping them with various ions.

The pulse-echo techniques are widely used for ultrasonic velocity measurement and elastic constants determination of various materials, such as PZT ceramics [1,2], PZN-PT single crystals [6,7], diamond, lanthanum aluminosilicate glasses, lanthanum gallogermanate glasses, triglycine sulfate single crystals, and other materials.

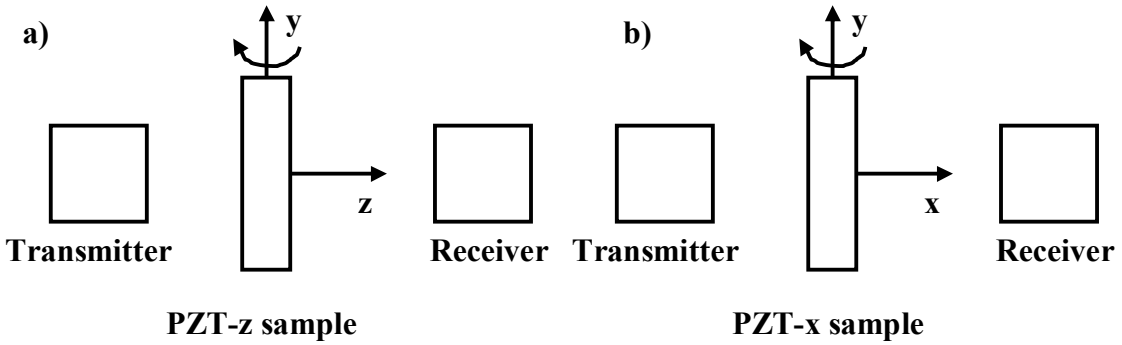

Fig. 1-1 Illustration of geometric relation between the transducer and sample. a) PZT-z and b) PZT-x samples used for measurement the phase velocity of the waves in the X-Z plane [1].

Fig. 1-1 shows the geometric relation between the transducer and sample, used for measurement of the phase velocity of the waves. The experimental setup, used for measurement of the phase velocities in the piezoelectric ceramics is shown in Fig. 1-2. Fig. 1-3 shows the phase velocity as a function of propagation direction in the XZ plane of a PZT-5H sample. The experimental data are shown as discrete points and the calculated results are shown as lines [1].

In [2], the ultrasonic velocities and dielectric constants were measured along different directions in the X-Z plane of a PZT ceramics (poling direction is along the Z-axis).

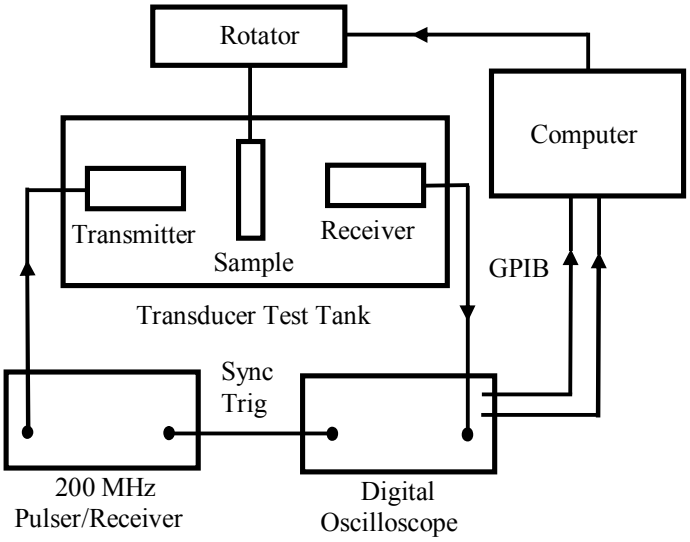

Fig. 1-2 Experiment setup for measurements the phase velocity as a function of propagation direction [1].

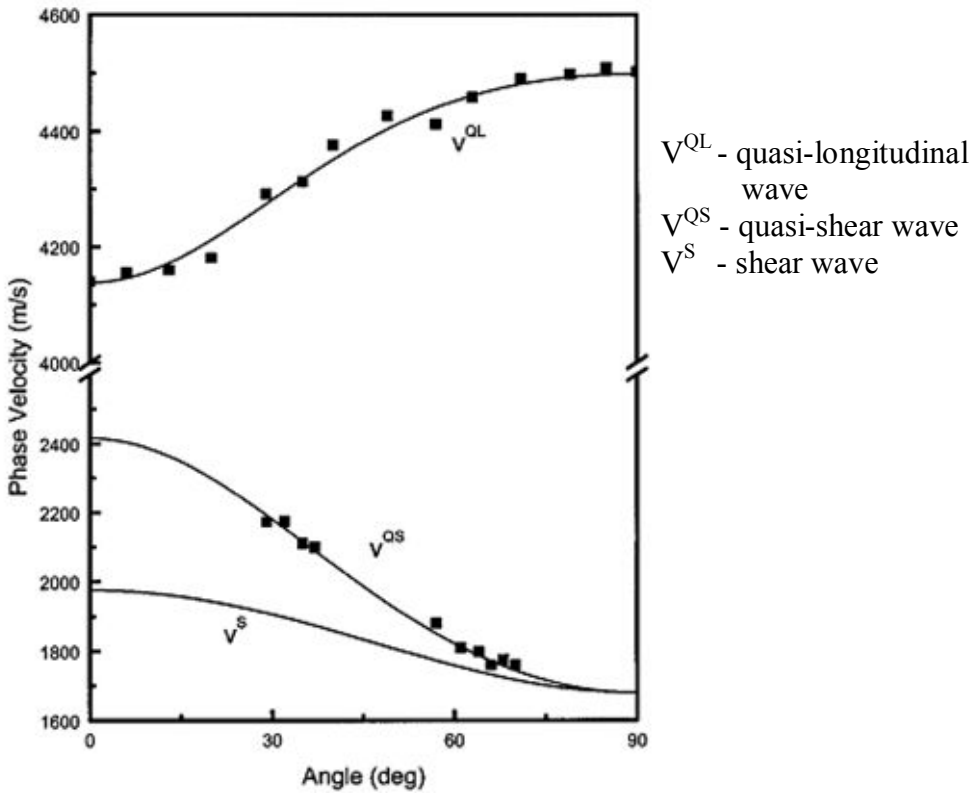

Fig. 1-3 The phase velocity of ultrasound wave as a function of propagation direction in the XZ plane of a PZT-5H sample. [1].

A complete set of values of the elastic stiffness constants and piezoelectric $e_{\lambda\mu}$- and $d_{\lambda\mu}$-constants has been obtained by the least squares method from the wave velocities and dielectric constants. Ceramic samples were poled by DC field, when the samples were cooled down from temperatures above the Curie temperature. The ultrasonic velocities were measured at room temperature by an ultrasonic pulse-echo overlap method using a Matec Pulse Modulator & Receiver Model 6600, a Decade Dividers & Dual Delay Generator Model 122B and a 5 MHz 0.5“ transducer (Harisonic Labs, Inc).

In [3], the dispersion of ultrasound velocity and attenuation for PZT ceramics were investigated by ultrasonic spectroscopy in the frequency range of 20-60 MHz. In the investigated frequency range, velocity dispersion of 1-3 m/s per MHz was observed.

In [4], phase velocities of ultrasound were used for characterization of the elastic properties of solids. The sample area should be much larger, than the size of the transducer, so that plane wave approximation holds. This geometric requirement is not possible to be realized for some materials, which can be made only in very small size. Using poled (under the electric field of 10 kV/cm for 3 min) and unpoled lead zirconate titanate (PZT-5H) ceramics as samples, have been analyzed experimentally to find any sample size influence on the ultrasonic measurements. The smallest dimension that is in contact with the transducer is only 14 % of the diameter of the transducer. The schematic geometry of the sample and the transducer arrangement are shown in Fig. 1-4. Figs. 1-5, 1-6 show the compensated ultrasonic wave phase velocities in poled and unpoled PZT-5H samples of different lateral dimensions. It was found, that the phase velocity increases, when the contact area becomes smaller. The velocity increase is 1.4 % and 0.9 %, respectively, in the unpoled and poled PZT-5H for the smallest dimension sample compared to bulk values. The relationship between d_{33} and the phase velocity on the same sample was measured and the results are shown in Fig. 1-7. All the measurements were performed on the same sample, which was depoled and repoled under different poling condition to obtain different d_{33} values. [4].

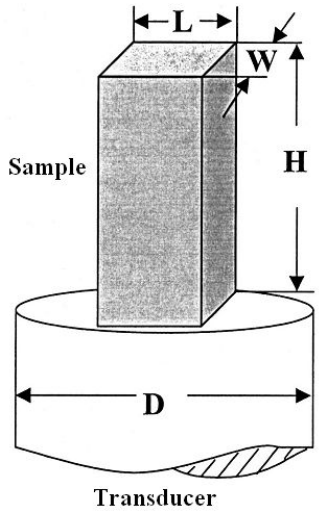

Fig. 1-4 Schematic geometry of the sample and transducer. The two lateral dimensions L and W were kept the same so that the cross section of the sample is maintained as a square [4].

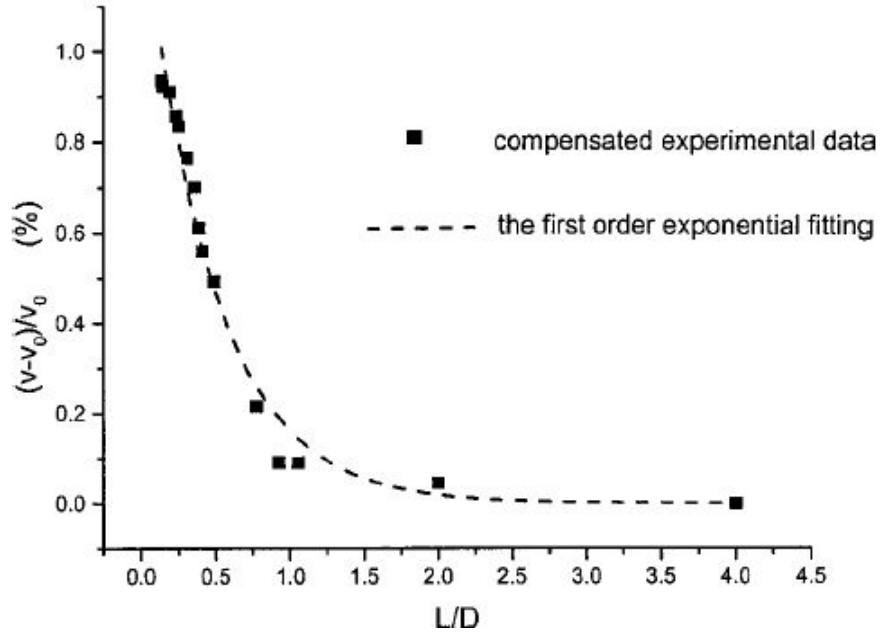

Fig. 1-5 Compensated ultrasonic wave phase velocities in poled PZT-5H samples of different lateral dimensions [4].

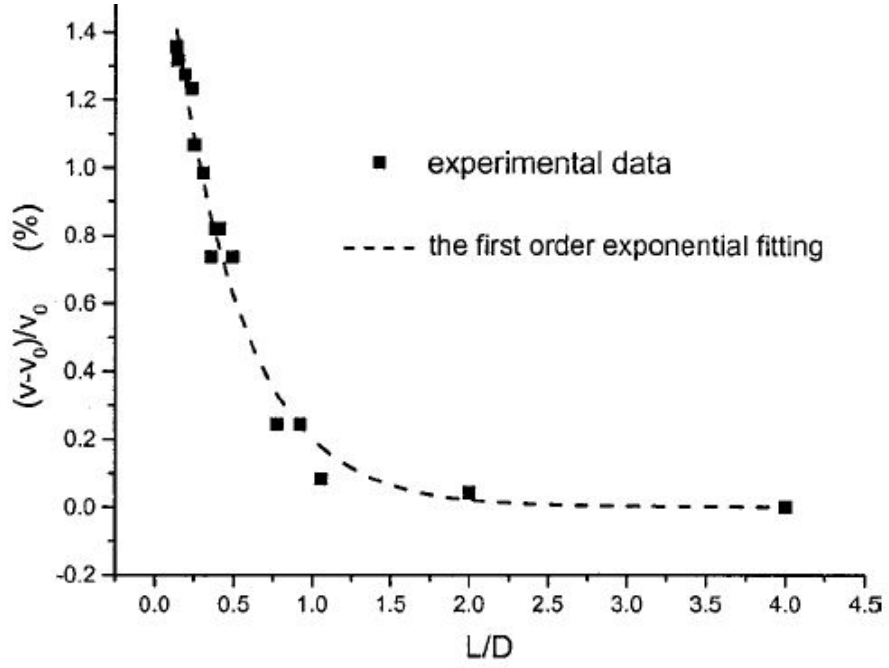

Fig. 1-6 Compensated ultrasonic wave phase velocities in unpoled PZT-5H samples of different lateral dimensions [4].

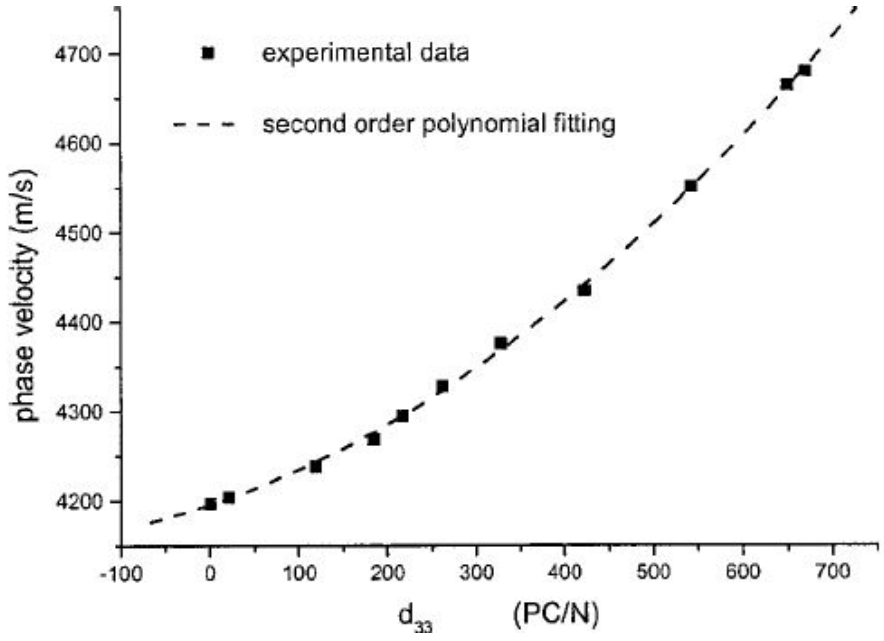

Fig. 1-7 The piezoelectric coefficient d_{33} vs. ultrasonic wave phase velocity measured on sample 1 [4].

Acoustic velocity and attenuation were measured in poled and unpoled lead zirconate titanate (PZT) ceramics, prepared by sintering and hot-pressing under different conditions. Hot-pressed PZT was found to have attenuation values approximately 1 order of magnitude smaller than sintered PZT. For both materials, poling caused a decrease in attenuation. Depolarization and phase transition phenomena were also observed at elevated temperatures, using a laser-ultrasound technique in combination with conventional pulse-echo measurements [5].

Relaxor based ferroelectric PZN-PT

The piezoelectric properties of $(1-x)Pb(Zn_{1/3}Nb_{2/3})O_3$-$xPbTiO_3$ (PZN-PT) and $(1-x)Pb(Mg_{1/3}Nb_{2/3})O_3$-$xPbTiO_3$ (PMN-PT) single crystals outperform the PZT series piezoelectric ceramics, leading to a revolution in electromechanical transducer technology. They have very high d_{33}, ranging from 2000 to 2500 pC/N, and the electromechanical coupling coefficient k_{33} is greater than 90 % [6], [7] and [8]. An ultrahigh k_{15}, up to 97 % have been reported in the shear-mode piezoelectric resonator of PMN-PT single crystal under an electric field applied along the $[1\bar{1}0]$ direction combined with a poling along the [111] direction [9].

There have recently been many research efforts directed at understanding polarization and its reorientation (switching) in relaxor single crystals. Ujiie and Uchino [10] observed domain reversal in relaxor ferroelectric PZN-PT under [111] electric field using a CCD microscope system. Noheda et al.'s experimental results make clear that once the crystal has been driven through the rhombohedral to tetragonal phase transition by application of a large electric field in the [001] direction, there was a permanent phase transition in the crystal. This was also suggested by Viehland's experimental results [11] which indicate a change of coercive field for 180° polarization reorientation after the material has been driven through the phase transition and back. Relaxor PZN-PT and PMN-PT single crystals display temperature and field dependent phase transformations [12, 13 and 14]. An electric field induced phase transition between a rhombohedral phase and a tetragonal phase has been reported [13 and 14].

Furthermore, Lu et al. [15] reported an observation of the orthorhombic ferroelectric phase in PZN-8%PT and PMN-33%PT single crystals. They found by optical observation, that a [110] oriented crystal could be poled to a [111] twinned multi-domain state (rhombohedral phase) or a [110] mono-domain state (orthorhombic phase).

In [16], the phase transitions in the relaxor ferroelectric PZN-4.5%PT in the temperature range 4.2-450 K were studied, using very high resolution neutron powder diffraction. Three phases, rhombohedral (*R*3*m*), tetragonal (*P*4*mm*) and cubic (*Pm*3*m*) were observed gradually in this range with increasing temperature. In [17] the properties of PZN-PT and PMN-PT single crystals of various compositions and orientations have been investigated. Transverse piezoelectric coefficient (d_{31}) of PZN-PT single crystals of various PT contents as functions of poling field was published. In [18] was presented the investigation of elastic, piezoelectric, and dielectric performances in $0.70Pb(Mg_{1/3}Nb_{2/3})O_3$-$0.30PbTiO_3$ (0.70PMN-0.30PT) single crystals using a resonance technique. The complete set of constants was determined for this [001]-poled domain-engineered system with the effective tetragonal *4-mm* symmetry.

The presence of a field-induced intermediate ferroelectric phase in pre-poled [111] oriented $0.955Pb(Zn_{1/3}Nb_{2/3})O_3$-$0.045PbTiO_3$ (PZN-4.5%PT) single crystals, was reported in [19]. The method of the measurement was based on the dielectric, differential scanning calorimetry and pyroelectric measurements. It was found that this phase exists in a very narrow interval of 4.3 °C between the ferroelectric rhombohedral and tetragonal phases. This may be explained as an electric-field-induced orthorhombic phase, what is based on previous investigations on the PZN-8%PT single crystals. An electric-field-induced phase diagram of [111] oriented PZN-PT has been redrawn based on this study.

The complete set of elastic, piezoelectric and dielectric constants of $0.92Pb(Zn_{1/3}Nb_{2/3})O_3$-$0.08PbTiO_3$ domain engineered single crystal were measured and presented in [20]. Both the ultrasonic pulse-echo and resonance methods were employed. The elastic stiffness constants c_{11}^E , c_{33}^D, c_{44}^E, c_{66}^E, c_{12}^E and c_{44}^D can be directly determined from the measurements of phase velocities of ultrasonic waves propagating along appropriate pure mode directions [21]. The elastic compliances s_{11}^E,

s_{33}^{E} and the electromechanical coupling coefficients, k_{33}, k_{31} and k_{t}, were determined from the measured resonance and anti-resonance frequencies of the length-extensional vibration bars and thickness-extensional vibration plate, respectively. Also, the piezoelectric strain constants d_{33} can be directly measured by using quasi-static method. The dielectric constants ε_{11}^{T} and ε_{33}^{T} were obtained from the low-frequency capacitances using the parallel plate capacitor approximation in [20].

Figs. 1-8 and 1-9 show the phase velocity dependence on the bias electric field. The measurements were realized on the $0.955Pb(Zn_{1/3}Nb_{2/3})O_3$-$0.045PbTiO_3$ samples. The attenuation depends nonlinearly on frequency and the shear wave exhibited an order of magnitude larger attenuation than the longitudinal one. Domain switching behavior of $0.955Pb(Zn_{1/3}Nb_{2/3})O_3$-$0.045PbTiO_3$ (PZN-PT) ferroelectric single crystal has been investigated, using the ultrasonic technique in addition to the polarization hysteresis measurements. The sound velocity changes drastically near the coercive field of the material, which reflects that domain rotation, occurred during polarization switching. A complete set of velocity versus electric field loops was measured quasi-statically in a switching cycle and compared with the polarization hysteresis loop [22].

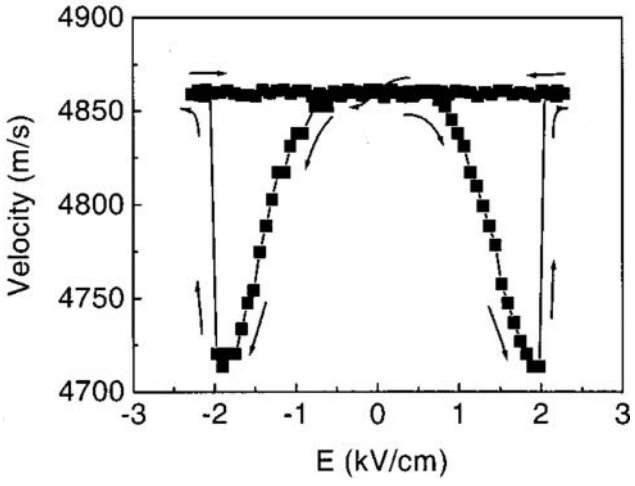

Fig. 1-8 Phase velocity along [111] under an electric field in the same direction [22].

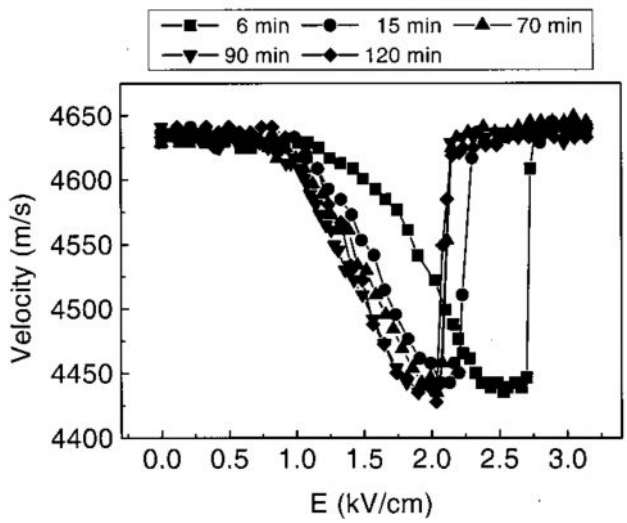

Fig. 1-9 *v –E* curves under an electric field applied during various times. Phase velocities were measured along $[0\bar{1}0]$ direction and the electric filed is applied along [111] [22].

Fig. 1-10(a) shows a loop of ultrasonic phase velocity versus electric field. For a comparison, a ferroelectric hysteresis loop obtained at the same time is also shown. The crystal sample was poled before the measurement so that the starting point is not the origin. The electric field was applied to the sample along the [111] direction of the cubic coordinates, or along the C axis of the trigonal coordinates, and the phase velocity of ultrasound in [111] direction was measured. The electric field is applied opposing the polarization at the beginning. When the field is gradually increased, the velocity is almost unchanged until the electric field amplitude reaches 0.6 kV/cm in negative field direction and 0.75 kV/cm in positive field direction. After this critical point, velocity begins to decrease with increasing field amplitude faster. The velocity reaches a minimum near the coercive field E_c and then drastically increases back to its original value with further increase of the field level.

Fig. 1-10(b) shows the velocity and the attenuation of ultrasound in the $[1\bar{1}0]$direction under an electric field in [111] direction (longitudinal wave with the propagation direction perpendicular to the field direction). Compared to the electric

hysteresis loop, one can see that the velocity minimum appears at the point of $P = 0$, $E = E_c$ [23].

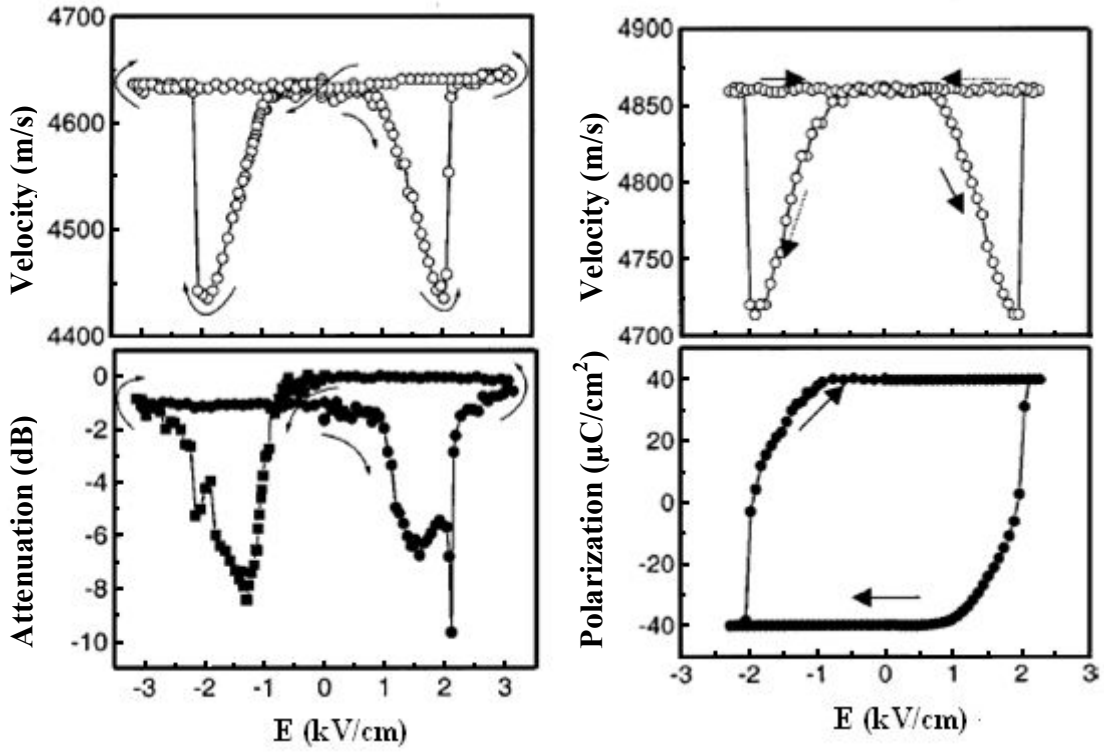

a) **b)**

Fig. 1-10 Velocity and attenuation versus electric field loops, polarization-electric field loop [23].

In [24], the sound velocities of longitudinal and shear waves along three pure mode directions [100], [001] and [110] of sample 1 and 2 were measured, using pulse-echo technique. A rectangular parallelepiped with dimensions along [100], [010], [001] (sample 1) and a rectangular parallelepiped with dimensions along [110], $[\bar{1}10]$, [001] (sample 2) were employed. Since shear waves could have their displacements parallel or perpendicular to the poling direction, it is possible to measure totally eight independent velocities in the three pure mode directions. The free dielectric permittivities ε_{11}^{T} and

ε_{33}^{T} are determined by capacitance measurements. A complete set of material constants is obtained by combined ultrasonic-resonance method using various samples.

Temperature-dependent measurements

In [25], the velocity of ultrasound in a group of lanthanum gallogermanate glasses was obtained by the ultrasonic pulse-echo measurements, at room temperature.

The temperature dependence of both longitudinal and transverse sound velocities of three lanthanum gallogermanate glasses is given in Fig. 1-11. The results indicate, that the ultrasonic velocities, both longitudinal and transverse, decrease slowly and monotonically with increasing temperature in the range of 25–350 °C. The variation of sound velocities has a small negative temperature coefficient.

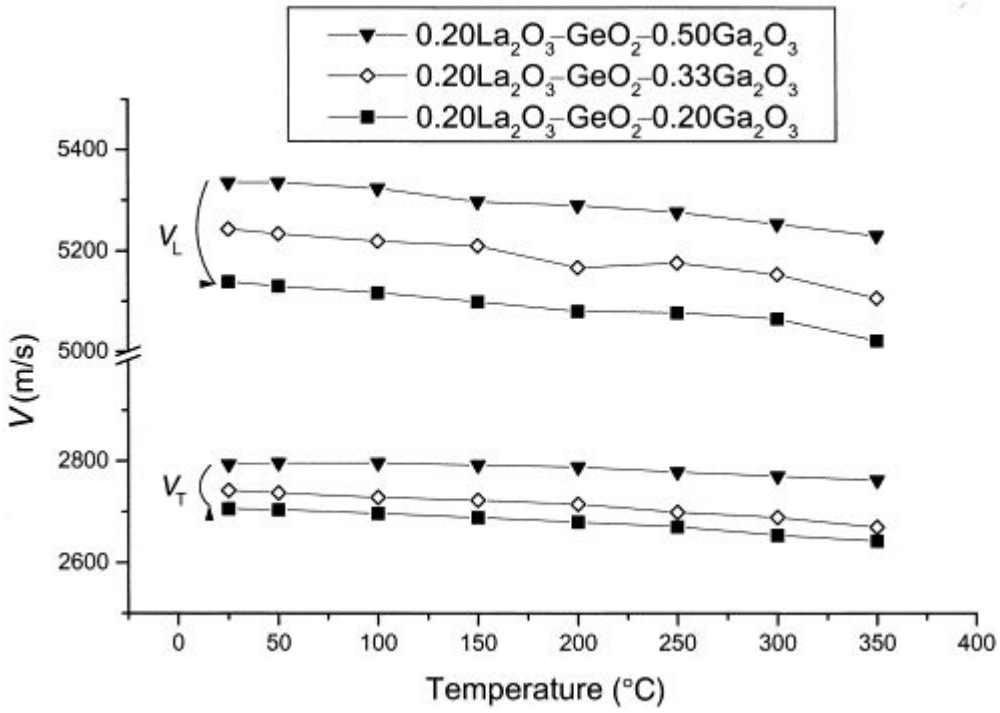

Fig. 1-11 The temperature dependence of both longitudinal and transverse sound velocities for a series of lanthanum gallogermanate glasses [25].

Both longitudinal and transverse waves velocities of these glasses depend on composition. The experimental results are used to obtain the elastic constants. The longitudinal ultrasonic attenuation and velocity were measured in triglycine sulfate (TGS) single crystal over the temperature range 30-100 ˚C. The results of these measurements are shown in Fig. 1-12. It was found that the peak of the relative ultrasonic attenuation near the second-order phase transition is lower in the heating process than that in the cooling process, and its height decreases with the increasing frequency. All experiments were carried out on a conventional pulsed spectrometer (MATEC 7700 series). The sample for experiments was 1 mm thick. A quartz transducer was bonded to the surface of the sample by silicon oil [26]

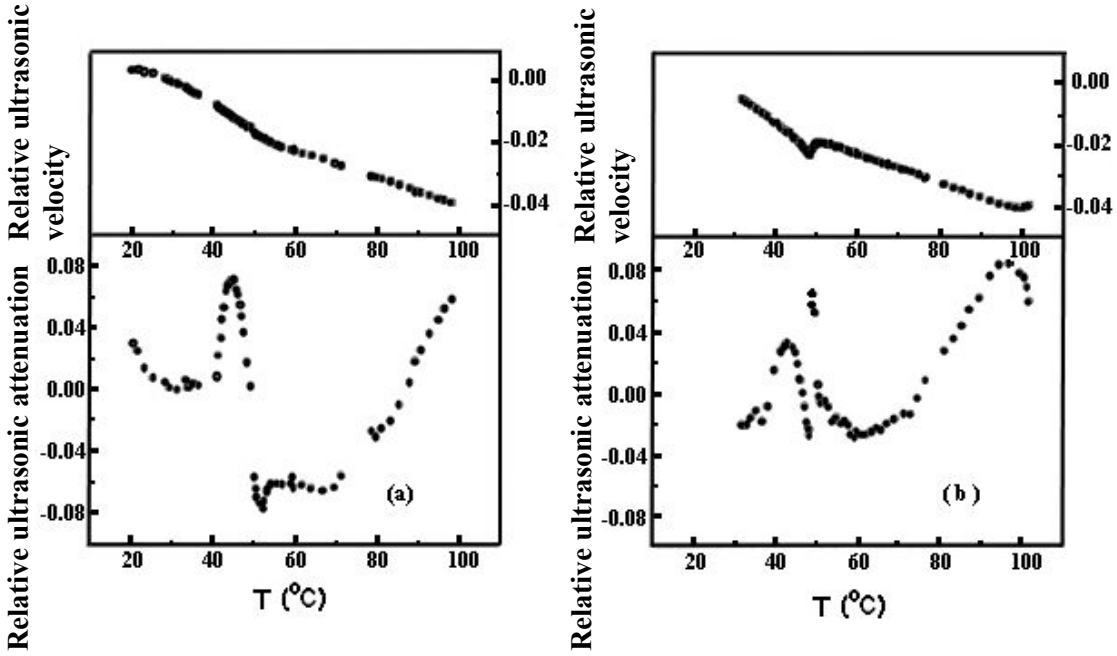

Fig. 1-12 Temperature dependence of relative ultrasonic attenuation and relative velocity in TGS single crystal at 5.56 MHz: (a) heating process, (b) cooling process [26].

The temperature dependence of elastic properties of a series of lanthanum gallogermanate glasses was determined by ultrasonic pulse-echo techniques. The measurements were performed on the Panametric model 5800 pulser/receiver, and

with two specially designed high temperature PZT transducers from Etalon Inc., in temperature up to 350 ˚C and at 20 MHz frequencies. X-cut transducers were employed for longitudinal modes and Y-cut for shear modes [27]. The velocity decreasing for longitudinal and shear waves was observed.

In [28] elastic properties of the filled skutterudite compounds $LaRu_4Sb_{12}$ and $PrRu_4Sb_{12}$ have been investigated by means of ultrasonic measurement. The sound wave velocity v was detected by an ultrasonic apparatus based on the phase-comparison method. Fig. 1-13 shows the temperature dependence of elastic constants c_{11}; $(c_{11} - c_{12})/2$ and c_{44} for $LaRu_4Sb_{12}$ and $PrRu_4Sb_{12}$. They all decrease monotonically with increasing temperatures.

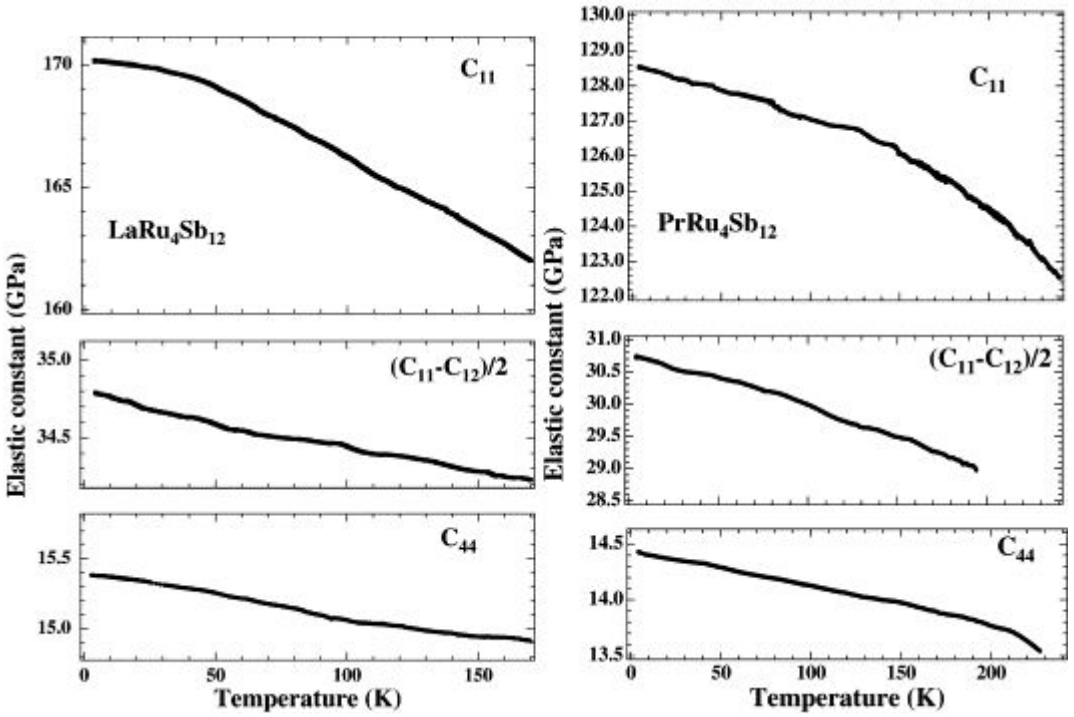

Fig. 1-13 Temperature dependence of elastic constants c_{11}, $(c_{11}-c_{12})/2$ and c_{44} for a) $LaRu_4Sb_{12}$ and b) $PrRu_4Sb_{12}$ [28].

1.2 Definition of the purposes and research problems

This work was focused on Lead Zirconate Titanate (PZT) ceramics and Lead Zinc Niobate-Lead Titanate (PZN-PT) single crystals. The primary purpose of this dissertation is to characterize an influence of the electric bias field on the elastic stiffness constants of above mentioned materials in temperature range from -50 °C up to 200 °C. These measurements are carried out for various crystal cuts of PZN-PT with various percentage amounts of PT. For these purposes, it is necessary to solve the following tasks:

- to propose the method for data processing of ultrasonic measurements;
- to develop the program for automatic recording of measured ultrasonic response from an oscilloscope and for measurement the time of flight of ultrasound waves through the sample;
- to design an appropriate sample holder;
- to develop the optimal method for the measurement under electric field in the thermal chamber.

Furthermore, it is necessary to discuss the possibilities, benefits and disadvantages of the ultrasonic methods and to interpret a different behavior and shapes of hysteresis loops for longitudinal and shear mode waves propagation under electric bias field at various temperatures.

2 Theoretical backgrounds

2.1 Wave Propagation

In solids, sound waves can propagate in four principle modes that are based on the way how particles oscillate. Sound can propagate as longitudinal waves, shear waves, surface waves, and in thin materials as plate waves. Longitudinal and shear waves are the two modes of propagation most widely used in ultrasonic testing. The particle movement responsible for the propagation of longitudinal and shear waves is illustrated in Fig. 2-1.

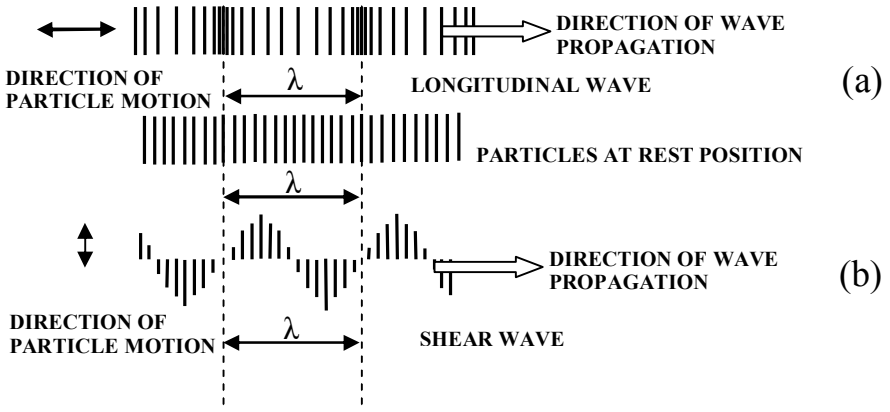

Fig. 2-1 Types of waves in bulk solid: (a) longitudinal waves, (b) shear waves.

In longitudinal waves, the oscillations occur in the longitudinal direction or the direction of wave propagation. In the transverse or shear wave, the particles oscillate at a right angle or transverse to the direction of propagation.

At cut-off frequency f_c, the group velocity V_g is zero because the tangent to the dispersion curve is horizontal. For frequencies well below the cut-off frequency, a crystal is non-dispersive for elastic waves, but it is anisotropic [29].

$$f_c = \frac{V_0}{\pi a}$$

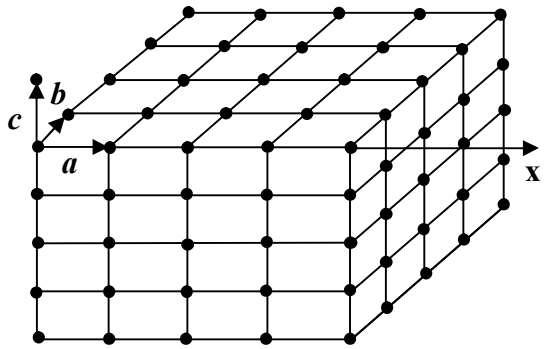

Fig. 2-2 Cubic crystal lattice structures and coordinates of atoms in such crystals.

More generally, the wave vector may be inclined to the vector ***a***. In this case there are still three waves that may propagate, but the atomic displacements are generally neither parallel nor perpendicular to the propagation direction. The wave with polarization closest to the propagation vector is called the quasi-longitudinal wave; the other two have polarizations perpendicular to this and are called quasi-transverse waves. In the particular case where the "springs" linking the atoms are identical for the direction ***b*** and ***c***, the two transverse waves with propagation along ***a*** have the same velocity. A propagation direction such as this is called an acoustic axis.

2.2 Christoffel Equation

If the solid has a disturbance propagating through it, the displacement u_i of an arbitrary point in the solid, with coordinates x_k varies with times, so that $u_i = u_i(x_k, t)$. The equation of motion follows from Newton's law [29]. Neglecting gravitation this equation to be

$$\rho \frac{\partial^2 u_i}{\partial t^2} = \frac{\partial T_{ij}}{\partial x_j} \tag{1}$$

In a piezoelectric medium, the coupling between the elastic field and the electromagnetic field introduces electrical terms into the development of Maxwell's equations. The distributions of these fields can in principle be determined only by simultaneously solving these coupled equations. In practice, since elastic fields involve displacements of the material, the velocity with which a stress or strain propagates is much less than that of an electric field. The velocity of elastic waves is 10^4 to 10^5 times smaller than the velocity of electromagnetic waves. Consequently, the magnetic field associated with mechanical vibrations plays little part; for example, the magnetic energy produced by a strain is negligible in comparison with the electrical energy. This implies that the electromagnetic field associated with an elastic field is quasi-static, so that Maxwell's equations reduce to:

$$\mathrm{rot}\vec{E} = -\frac{\partial \vec{B}}{\partial t} \approx 0\,, \text{ giving} \qquad \vec{E} = \text{-grad}\,\Phi$$

The linear equation of state [29]

$$T_{\mathrm{jk}} = c^{E}_{\mathrm{jklm}} S_{\mathrm{lm}} - e_{\mathrm{ijk}} E_{\mathrm{i}} \tag{2}$$

$$D_{\mathrm{j}} = e_{\mathrm{jkl}} S_{\mathrm{kl}} + \varepsilon^{S}_{\mathrm{jk}} E_{\mathrm{k}}$$

Substituting for the strain $S_{\mathrm{kl}} = \frac{1}{2}\left(\frac{\partial u_{\mathrm{l}}}{\partial x_{\mathrm{k}}} + \frac{\partial u_{\mathrm{k}}}{\partial x_{\mathrm{l}}}\right)$ and the electric field $E_{\mathrm{k}} = -\frac{\partial \Phi}{\partial \mathrm{x}_{\mathrm{k}}}$ into (2) this becomes

$$T_{\mathrm{ij}} = c^{E}_{\mathrm{ijkl}} \frac{\partial u_{\mathrm{l}}}{\partial x_{\mathrm{k}}} + e_{\mathrm{kij}} \frac{\partial \Phi}{\partial x_{\mathrm{k}}}, \tag{3}$$

Hence Newton's law, in the form of (4), becomes

$$\rho \frac{\partial^2 u_{\mathrm{i}}}{\partial t^2} = c^{E}_{\mathrm{ijkl}} \frac{\partial^2 u_{\mathrm{l}}}{\partial x_{\mathrm{k}} \partial x_{\mathrm{j}}} + e_{\mathrm{kij}} \frac{\partial^2 \Phi}{\partial x_{\mathrm{k}} \partial x_{\mathrm{j}}} \tag{4}$$

Moreover, the electric displacement is

$$D_{\mathrm{i}} = e_{\mathrm{jkl}} \frac{\partial u_{\mathrm{l}}}{\partial x_{\mathrm{k}}} - \varepsilon^{S}_{\mathrm{jk}} \frac{\partial \Phi}{\partial x_{\mathrm{k}}} \tag{5}$$

And for the insulating solid this must satisfy Poisson equation $\frac{\partial D_{\mathrm{j}}}{\partial x_{\mathrm{j}}} = 0$, so that

$$e_{\mathrm{jkl}} \frac{\partial^2 u_{\mathrm{l}}}{\partial x_{\mathrm{j}} \partial x_{\mathrm{k}}} - \varepsilon^{S}_{\mathrm{jk}} \frac{\partial^2 \Phi}{\partial x_{\mathrm{j}} \partial x_{\mathrm{k}}} = 0 \tag{6}$$

The wave equation for the displacement u_{i} is obtained by eliminating the potential Φ between (4) and (6). For a plane wave propagating along the direction $\vec{\mathrm{n}}$, solution for u_{i} and Φ have the forms

$$u_{\mathrm{i}} = \mathrm{v}_{\mathrm{i}} F(t - \frac{n_{\mathrm{j}} \cdot x_{\mathrm{j}}}{V}), \qquad \Phi = \Phi_0 \cdot F(t - \frac{n_{\mathrm{j}} \cdot x_{\mathrm{j}}}{V}) \tag{7}$$

Each wavefront is an equipotencial, so that the electric field is longitudinal, being given by

$$E_{\mathrm{j}} = -\frac{\partial \Phi}{\partial x_{\mathrm{j}}} = \frac{n_{\mathrm{j}}}{V} \cdot \Phi_0 \cdot F',$$

where F' is the derivative of the function *F*.

Substituting (7) into (4) and (6) gives the relations

$$\frac{\partial^2 u_i}{\partial t^2} = v_i \cdot F'', \qquad \frac{\partial^2 u_l}{\partial x_j \partial x_k} = \frac{n_j n_k}{V^2} \cdot v_l \cdot F'', \qquad \frac{\partial^2 \Phi}{\partial x_j \partial x_k} = \frac{n_j n_k}{V^2} \cdot \Phi_0 \cdot F''$$

Defining the quantities:

$$\Gamma_{il} = c^E_{ijkl} n_j n_k, \qquad \gamma_i = e_{kij} n_j n_k, \qquad \varepsilon = \varepsilon^S_{jk} n_j n_k, \tag{8}$$

the above leads to the system of equations:

$$\rho V^2 \cdot v_i = \Gamma_{il} \cdot v_i + \gamma_i \cdot \Phi_0 \tag{9}$$

$$\gamma_l \cdot v_l - \varepsilon \cdot \Phi_0 = 0$$

On eliminating the electric potential Φ_0, this leads to

$$\rho V^2 \cdot v_i = \left(\Gamma_{il} + \frac{\gamma_i \gamma_l}{\varepsilon} \right) \cdot v_l \tag{10}$$

As for a non-piezoelectric solid, the polarizations v_i of the plane elastic waves propagating in chosen direction, are the eigenvectors of tensor of rank two, defined in this case by

$$\bar{\Gamma}_{il} = \Gamma_{il} + \frac{\gamma_i \gamma_l}{\varepsilon}, \tag{11}$$

And the eigenvalues $\bar{\gamma} = \rho \cdot V^2$ give the phase velocities. The polarizations of the three waves are always mutually orthogonal, since the tensor $\bar{\Gamma}_{il}$ is symmetric.

The influence of piezoelectricity on the phase velocity can be expressed in term soft modified stiffness constants of the material. As for a non-piezoelectric solid, the Christoffel tensor can be written in the form

$$\bar{\Gamma}_{il} = \bar{c}_{ijkl} n_j n_k, \quad \varepsilon = \varepsilon^S_{jk} n_j n_k$$

Where the $\bar{c}_{ijkl}$ are effective constants defined by

$$\bar{c}_{ijkl} = c^E_{ijkl} + \frac{\left(e_{pij} n_p\right) \cdot \left(e_{qkl} n_q\right)}{\varepsilon^S_{jk} n_j n_k} \tag{12}$$

The constants $\bar{c}_{ijkl}$, called „stiffened“ constants, are not true elastic constants, since they are defined only for plane waves and they depend on the propagation direction [29, 34].

3. Experimental setup

3.1 Measurement of phase velocity and attenuation

It is difficult to use the resonance technique for determination of the physical properties of piezoelectric materials for some low symmetry systems, because several samples are needed and the degree of poling depends on sample geometry. The ultrasonic method on the other hand, allows the determination of a complete set of elastic, piezoelectric, dielectric constants for materials of certain symmetries. However, some of these independent constants can't be directly measured from the phase velocities of pure modes; they need to be derived by solving complicated coupled Christoffel equations.

Two different types of velocity measurement are generally required. Absolute measurements are needed, mainly to determine elastic constants when combined with the density. Relative velocity measurements are used to monitor relatively small changes in velocity with variation of external parameters such as pressure or temperature. Great care must be taken for velocity measurements is dispersive media. In this case, time of flight measurements always give the group velocity while special phase comparison techniques are needed to measure the phase velocity. We assume that $V_p = V_g = V$. Than the velocity can be obtained by simple time of flight measurement between selected echoes.

Attenuation is much more difficult to determine than velocity, and the absolute attenuation of a sample is sample dependent and sensitive to the presence of small and usually poorly characterized defects.

The phase velocity V of the wave can be generally expressed as a ratio of the thickness d of the sample and time of flight τ of the ultrasonic echoes, which are generated by reflections at a pair of parallel surfaces of the sample. The linear function of times of flights on order of response *i* is used to get the averaged velocity $\overline{V}$ from response spectrum in Fig. 3-1:

$$t_{i+1} = t_i + \delta\tau \cdot i, \qquad i = 1, 2...n \qquad\qquad \overline{V} = \frac{2d}{\delta\tau} \tag{13}$$

Fig. 3-1 shows a train of echoes from multiple round-trips through the PZT sample. The time $\delta\tau$ between two successive echoes is the time required for the pulse to travel through the sample and back to the transducer.

The relative attenuation coefficient α can be generally expressed in standard units as

$$\alpha = -\ln\frac{A_{n+1}}{A_n}\Big/2d \quad \left[neper \cdot m^{-1}\right] \text{ or in other units } -10\log\frac{A_{n+1}}{A_n}\Big/2d \quad \left[dB \cdot m^{-1}\right] \tag{14}$$

where $2d$ is the travel distance of the wave, i.e. for one transducer method it is thickness of the sample multiplied by two, and A_i is the magnitude of i-th echo response.

The value of relative attenuation α equals tangent of a linear function (14) $\ln\frac{A_{n+1}}{A_n}$ vs. travel distance $2d$, see Fig. 3-2.

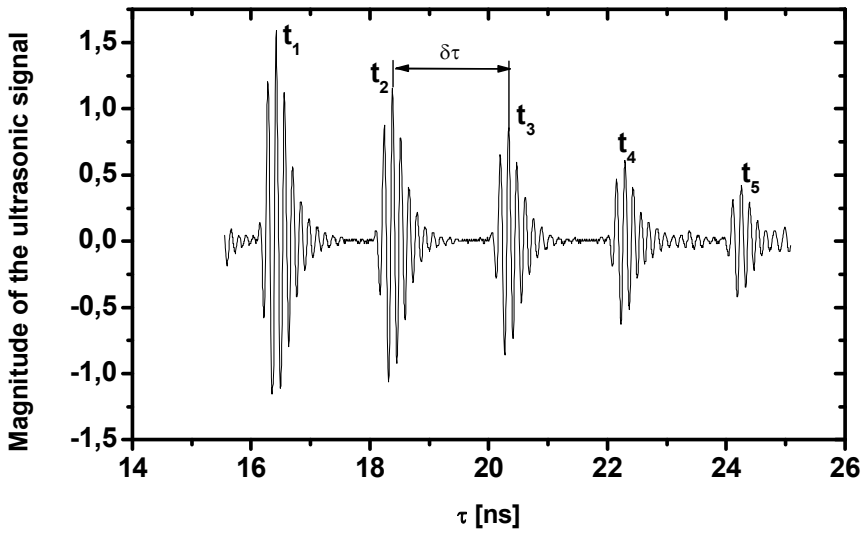

Fig. 3-1 The response of shear ultrasonic wave for PZT ceramics.

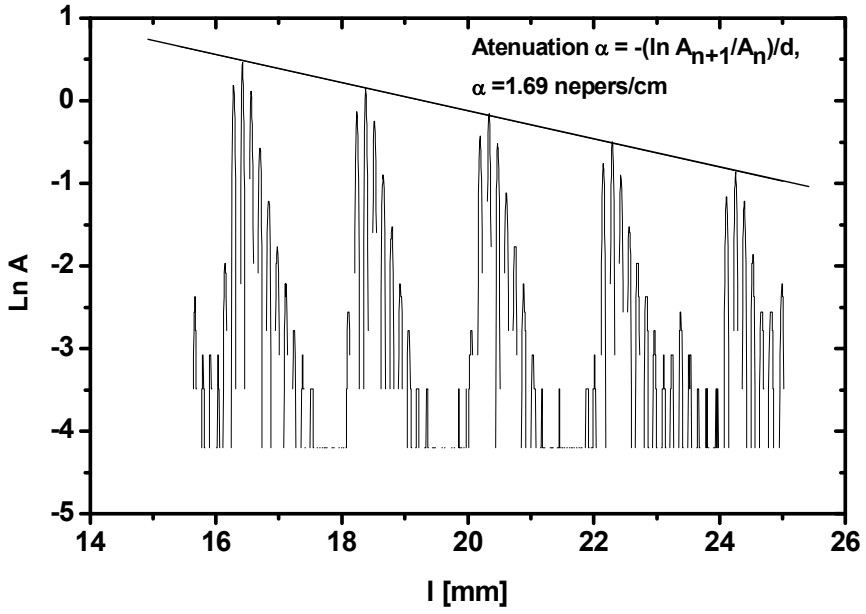

Fig. 3-2 The logarithmic response of PZT ceramics. The slope of the solid line is proportional to attenuation coefficient α.

3.2 Special requirements on devices for the ultrasonic measurements

For generation of ultrasonic waves, the transducers, vibrating in thickness-longitudinal or thickness-transverse mode, are often used. It is possible to generate and detect an ultrasound in a contact way in frequency range 10^5 - 10^{11} Hz. From equation of motion, wave equations and appropriate border and initial conditions, it is possible to determine the oscillation mode and the equivalent electrical scheme of the transducer. The ultrasound piezoelectric transducers may be used as well for non-destructive material testing, as for the determination of an ultrasound wave velocity propagation and attenuation in an investigated material. The transducer works as a transmitter or receiver, or performs both functions at the same time in so-called single-transducer mode.

Ultrasonic transducer has to satisfy some requirements:

1. Maximum possible transmitting pulsed performance of ultrasonic transducer under minimum pulse width.
2. Sufficient sensitivities for receiving weak short pulses.
3. Sufficient ratio of operating signal to signals parasitic, rising in the transducer.
4. Good resolution.
5. Minimum dead zone in the case of single-transducer mode, when the same transducer works as a transmitter and as a receiver of ultrasonic impulses.
6. The possibility of good acoustic contact with surface of the material that is examined.
7. Matching acoustical impedance on environment (to the material that is examined).
8. Optimum pattern.

3.3 Characteristics of Piezoelectric Transducers

The transducer incorporates a piezoelectric element, which converts electrical signals into mechanical vibrations (transmitting mode) and mechanical vibrations into electrical signals (receiving mode). Many factors, including material, mechanical and electrical constructions, and the external mechanical and electrical loads conditions, influence the behavior a transducer. Mechanical construction includes parameters such as radiation surface area, mechanical damping, housing, connector type and other characteristics of physical construction.

Fig. 3-3 shows a schematic diagram of an ultrasonic contact transducer. The primary component is the piezoelectric quartz crystal, which converts a mechanical pulse into an electrical signal, or conversely, an electrical signal to a mechanical pulse. In the pulse-echo method, the crystal functions in both modes. According to the manner in which the piezoelectric crystal is cut, it vibrates in the thickness direction, producing longitudinal waves, or in the tangential direction producing shear waves.

Between the contact transducer and the specimen, a coupling medium is used. It is necessary because the acoustic impedance mismatch between air and solids. The acoustic impedance of the test specimen is large and, therefore, nearly all of the energy is reflected and very little is transmitted into the test material. The most

common coupling material used for longitudinal waves, is glycerin, which is non-toxic and washes off by water. It is more difficult to transmit shear waves across the transducer/specimen interface, so a high viscosity coupling material is more effective.

Removable delay line can make a single transducer effective for a wide range of applications. The primary function of a delay line transducer is to introduce a time delay between the generation of the sound wave and the arrival of any reflected waves.

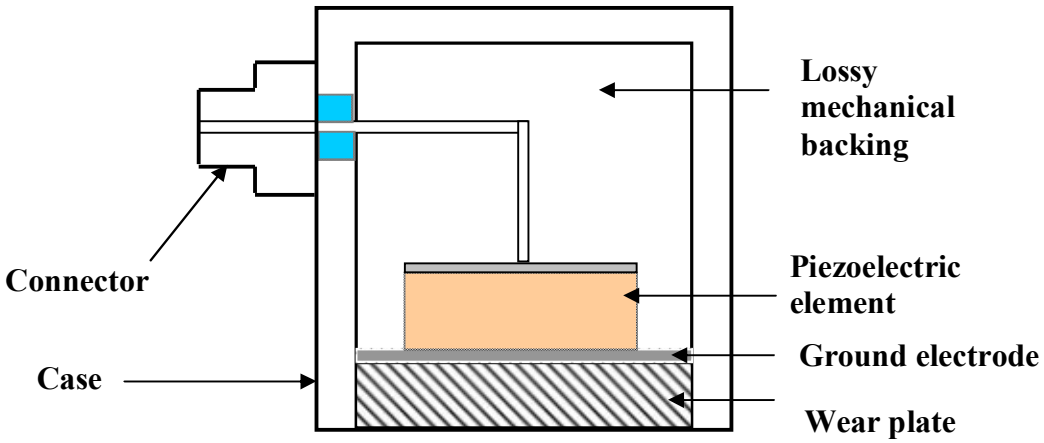

Fig. 3-3 Construction of an ultrasonic transducer.

This allows the transducer to complete its "sending" function before it starts its "listening" function so that near surface resolution is improved.

Ultrasonic transducers have many critical specifications [30]:

- Transmitting frequency – the usable frequency range of the device.
- Bandwidth – the difference between low and high operational frequency limits. Rated signal power available from transducer is another important specification.
- Transmitting sensitivity – the ratio of sound pressure produced, to input voltage.
- Receiving sensitivity – the ratio of output voltage produced, over sound pressure sensed.
- The beam angle – the total included angle of ultrasonic beam.

In general, a high frequency transducer will produce a narrow beam and a lower frequency transducer a wider beam. The beam angle can be influenced somewhat by the transducer housing construction.

Requirements to transmission of narrow pulse, good resolution and small dead zone are correlated and determined by correlation of transferred frequency band and middle frequency: $\Delta f / f_s$, where f_s is middle frequency of transducer, that can be determined by the length of single high-frequency oscillations, that form the impulse.

The boundary frequency of band $f_d - f_h = \Delta f$ is that, that make amplitude spectrum go down for about 3 dB in relation to the middle frequency. For reflex method, when the same transducer serves for transmission and for reception ultrasonic impulses, the decrease of amplitude spectrum on zone limits is –6 dB [30].

Limitation

- Materials that are rough, irregular in shape, very small, exceptionally thin or not homogeneous are difficult to inspect.

Dependence of ultrasound wave propagation on type of ultrasonic transducer.

Depending on purpose, it is possible to use one or two transducers, use delay lines or angular transducers for measurement of the time responses, see. Fig. 3-4. We can distinguish several methods:

1. The passageway method so-called „ Through Transmition", cases *a*, *b*, is most effective system, especially used for modern composite materials and other highly damping materials.
2. Reflex method with one transducer, case *d*. The disadvantage of this method is possibility of overloading the transducer with the generation pulse.
3. Modification using delay line so-called “buffer stock”, which get out disadvantages of reflex method, case *c*.
4. „Pitch and Catch” systems use two transducers with angular elements, case *e*.

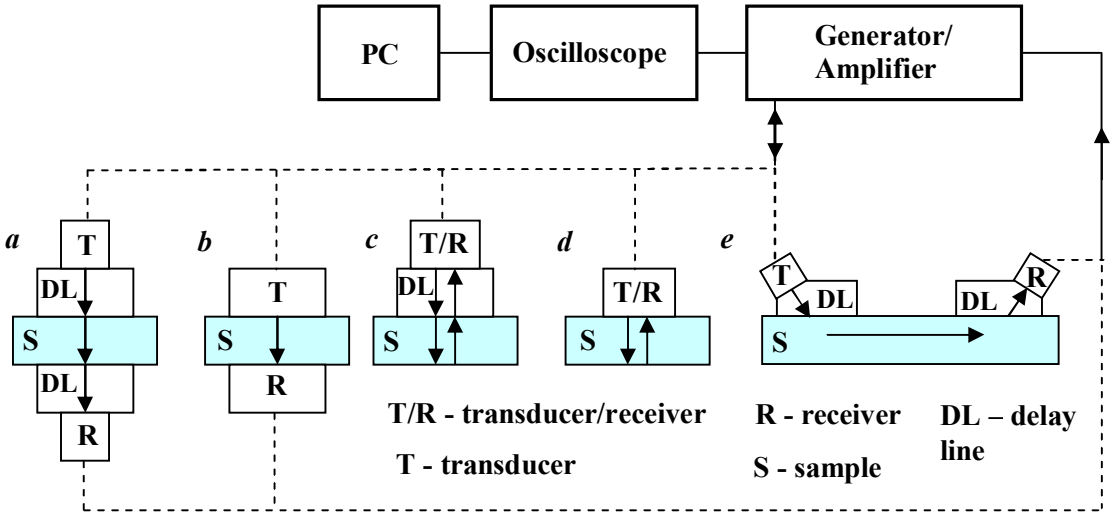

Fig. 3-4 Experimental setup for pulse/tone burst tones: a) transmission method with double delay line, b) transmission method, c) reflection method with delay line, d) reflection (echo) methods, e) transmission method for studies of surface waves.

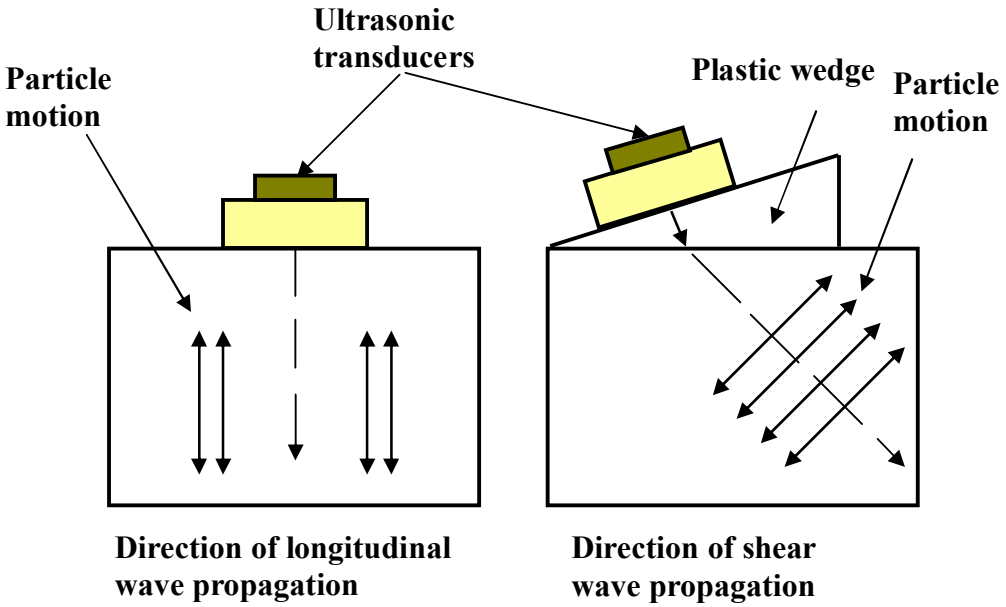

Fig. 3-5 The application of various transducers and delay lines for generating ultrasonic waves with different directions of propagation and polarizations.

The transducers with plastic wedge or specially designed so-called angular transducers for providing of the wave propagation in an angle given by Snell's Law in general direction are sometimes also used. Fig. 3-5 shows measurement of ultrasound wave velocity propagation using different transducers and delay lines.

3.4 Equipment

The ultrasonic pulse-echo technique was used. The ultrasonic system is based on Matec Instruments, Inc. modules. The time domain response was recorded and time of flight between echoes was directly measured by digital oscilloscope, type Agilent 54622D. The high bias field was applied on disk samples by the high voltage amplifier type Trek 610D, using a special setup and sample holder.

Equipment

1) Pulse Modulator & Receiver (Model 7700) (pulsed spectrometer).
2) Decade Dividers & Dual Delay Generator (Model 122B).
3) Master synchronizer & exponential generator (Model 1204A).
4) High frequency oscilloscope (Agilent 54622D).
5) Frequencies counter (HP5384A).
6) High resolution frequency source (Model 110).
7) Commercial Lithium Niobate transducers (Valpey Fisher, type DP152 - 0.25" with polystyrene delay and SD152-FL with fused silica delay) with fundamental frequency 15 MHz for longitudinal and shear wave.
8) Shear wave transducer 7x14 mm^2, $LiNbO_3$, with metallic coupling layer to glass delay line working on 22 MHz.
9) Transducer cable.

The ultrasound velocities were measured using the experimental setup as shown in Fig. 3-6. The Pulse Modulator & Receiver Model 7700 generated the tone burst pulses and the Plug-in Model 755, 0.5 – 22 MHz, received R.F. echoes. The electric DC

bias field was applied by HV amplifier Trek model 610D. The time domain response was recorded and time of flight between echoes directly measured by digital oscilloscope, type Agilent 54622D. A pulse echo-overlap technique was used for the determination of the absolute values of velocity, with which the high precision - better than 1 % can be obtained.

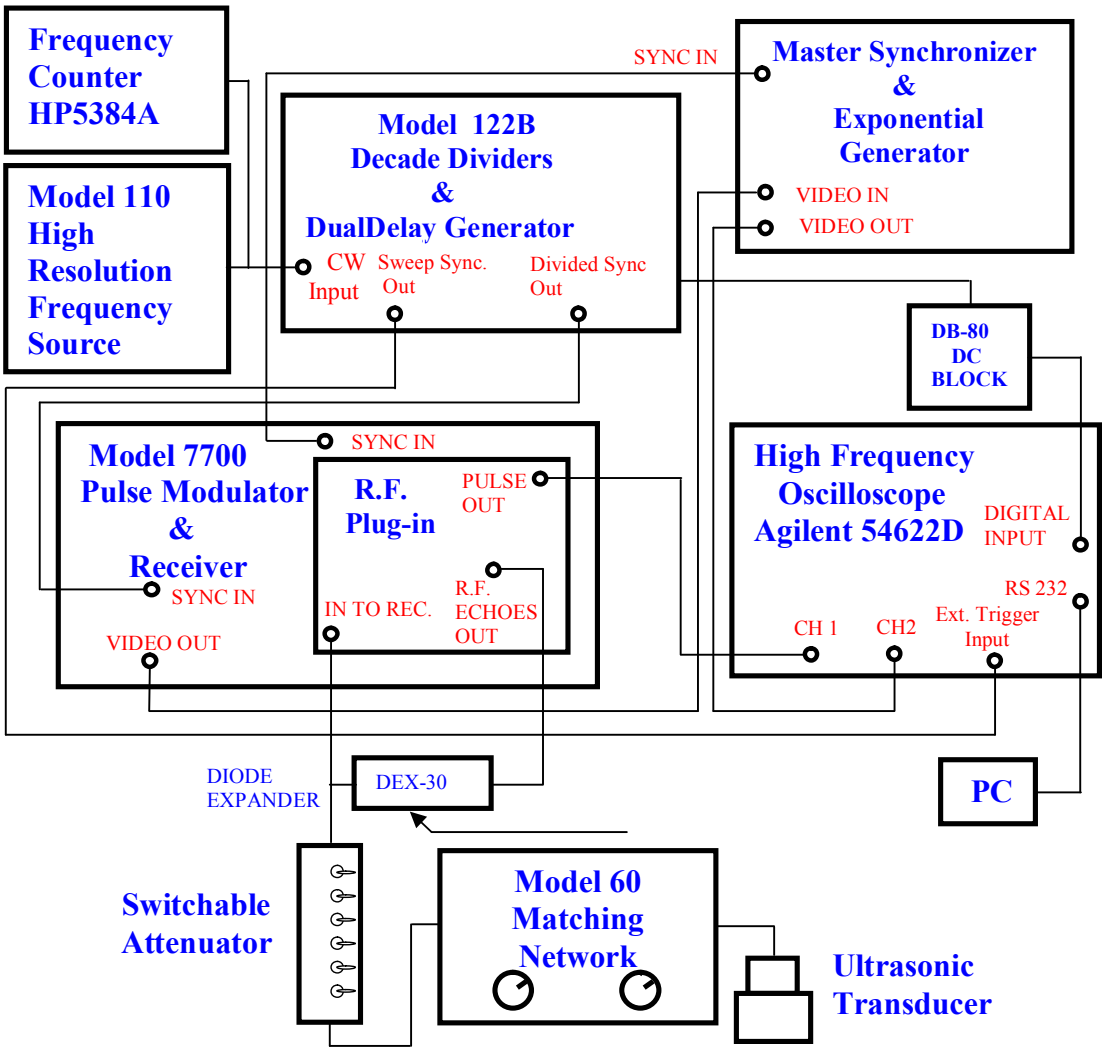

Fig. 3-6 Experimental setup for ultrasonic measurement.

Synchronizer

Synchronizer is a generator of triggers in adjusted repeating frequency f_0 that will start time-base generator at time t_0. There is a delay circuit either in synchronizer, generator, or in the time base source. Its purpose is to form the next start pulse that is delayed for some time t_1, for initial impulse of generator not to be directly at the beginning of the time base, but with definite distance.

The received signals transfer through the attenuator, where they are adjusted to desirable height or rate. Attenuator doesn't change mutual correlation of echoes, because it is consisted only of passive elements. We get in its exit either high-frequent impulse after amplification in the amplifier, or video impulses after rectification and filtration [30].

Generator

Generator is an electric circuit that actuates the electro acoustic transducer to send out ultrasonic impulse. In general, generators may be divided into 2 types: with tank circuit and without tank circuit. Generators with tank circuit transmit impulses with narrow or standard bandwidth, while untuned generators are use to actuate broadband sounds with a very narrow pulse. Impulses that are used to investigate material have mainly exponential form of envelope curve; they are damped oscillations. Their advantage is the high-pitched start.

Amplifier

In the pulsed devices, more often the linear amplifiers are used. The voltage on their output is directly proportional to the signal on its entrance [30].

In the pulse-echo ultrasonic system, an ultrasound transducer generates an ultrasonic pulse and receives its „echo". The ultrasonic transducer functions as both transmitter and receiver in one unit. Most ultrasonic transducer units use an electronic

pulse to generate a corresponding sound pulse, using the piezoelectric effect. A short, high voltage electric pulse (less than 20 ns in duration, 100-200 V in amplitude) excites a piezoelectric crystal, to generate an ultrasound pulse. The transducer broadcasts the ultrasonic pulse at the surface of the specimen. The ultrasonic pulse travels through the specimen and reflects off the opposite face. The transducer then „listens“ to the reflected echoes. The ultrasound pulse keeps bouncing off the opposite faces of the specimen, attenuating with time.

Procedure of measurement:

1. Measurements of the dimensions of the sample in the directions through which we will send the ultrasound.
2. Holding up the transducer against the sample using a small amount of the honey.
3. Making accurate measurements of the time between the first echo and the second echo using the cursors of the oscilloscope.
4. The calculations of an ultrasonic shear and longitudinal velocities and attenuation.

A pulse echo-overlap technique was used for the determination of the absolute velocity values. This technique allows absolute velocities to be obtained with high precision (0.01 %). The experimental results can be used to obtain the elastic and piezoelectric coefficients. The values of elastic coefficient, derived from experimental data for these samples, can be compared with the resonance measurements. From this it can be seen, that some elastic coefficient are approximately the same for both resonance and ultrasound methods.

The measurement of PZT samples under DC bias electric field was realized inside the special sample holder, see Fig. 3-7.

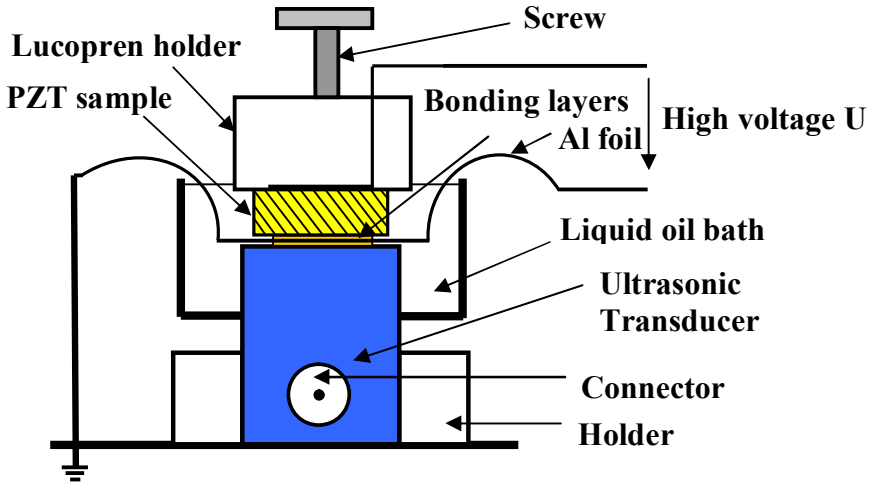

Fig. 3-7 A sample-holder for measurements of PZT ceramic samples under high voltage DC bias.

4. Experimental Results

4.1 Simulation by MathCAD

The relationships between the measured ultrasonic phase velocities and related elastic constants were derived from the Christoffel wave equations for various directions of ultrasonic wave propagation, and these relationships have been expressed using MathCAD v.13.0 and are shown in Fig. 4-1 up to Fig. 4-6. MathCAD is an applied mathematics program, enabling scientists to perform the most complex calculations, and edit scientific and technical documentation at the same time.

$$c6mm=\begin{pmatrix} c_{11} & c_{12} & c_{13} & 0 & 0 & 0 \\ c_{12} & c_{11} & c_{13} & 0 & 0 & 0 \\ c_{13} & c_{13} & c_{33} & 0 & 0 & 0 \\ 0 & 0 & 0 & c_{44} & 0 & 0 \\ 0 & 0 & 0 & 0 & c_{44} & 0 \\ 0 & 0 & 0 & 0 & 0 & \frac{c_{11}-c_{12}}{2} \end{pmatrix} \quad \varepsilon 6mm=\begin{pmatrix} \varepsilon_{11} & 0 & 0 \\ 0 & \varepsilon_{11} & 0 \\ 0 & 0 & \varepsilon_{33} \end{pmatrix}$$

$$d6mm=\begin{pmatrix} 0 & 0 & 0 & 0 & d_{15} & 0 \\ 0 & 0 & 0 & d_{15} & 0 & 0 \\ d_{31} & d_{31} & d_{33} & 0 & 0 & 0 \end{pmatrix}$$

Fig. 4-1 Matrixes of piezoelectric coefficient $d_{i\lambda}$, elastic module c and permittivity ε for *6mm* symmetry.

Direction of propagation:

$$\theta=\frac{\pi}{2},\ \phi=0,\ n=\begin{pmatrix} \sin\theta\cdot\cos\phi \\ \sin\theta\cdot\sin\phi \\ \cos\theta \end{pmatrix}$$

Choice of symmetry: $dp=d6mm$ $c=c6mm$ $\varepsilon 1=\varepsilon 6mm$

The direction of ultrasound wave propagation in a system of Cartesian axes:

$$n=\begin{pmatrix}1\\0\\0\end{pmatrix}$$

Calculation of piezoelectric matrix *e*: $ep=dp\cdot c6mm$

$$ep=\begin{pmatrix}0 & 0 & 0 & 0 & d_{15}\cdot c_{44} & 0\\ 0 & 0 & 0 & d_{15}\cdot c_{44} & 0 & 0\\ d_{31}\cdot c_{11}+d_{31}\cdot c_{12}+d_{33}\cdot c_{13} & d_{31}\cdot c_{11}+d_{31}\cdot c_{12}+d_{33} & 2d_{31}\cdot c_{13}+d_{33}\cdot c_{33} & 0 & 0 & 0\end{pmatrix}$$

Fig. 4-2 Calculation of piezoelectric matrix ***e***.

Calculation of piezoelectric matrix γ:

$$\gamma=\begin{pmatrix}ep_{0,0}(n_0)^2+ep_{1,5}(n_1)^2+ep_{2,4}(n_2)^2+(ep_{0,5}+ep_{1,0})n_0n_1+\\+(ep_{0,4}+ep_{2,0})n_0n_2+(ep_{1,4}+ep_{2,5})n_1n_2\\ ep_{0,5}(n_0)^2+ep_{1,1}(n_1)^2+ep_{2,3}(n_2)^2+(ep_{0,1}+ep_{1,5})n_0n_1+\\+(ep_{0,3}+ep_{2,5})n_0n_2+(ep_{1,3}+ep_{2,1})n_1n_2\\ ep_{0,4}(n_0)^2+ep_{2,2}(n_2)^2+ep_{2,2}(n_2)^2+(ep_{0,3}+ep_{1,4})n_0n_1+\\+(ep_{0,2}+ep_{2,4})n_0n_2+(ep_{1,2}+ep_{2,3})n_1n_2\end{pmatrix}=\begin{pmatrix}0\\0\\d_{15}c_{44}\end{pmatrix}$$

Fig. 4-3 Calculation piezoelectric matrix ***γ***.

Christoffel matrix:

$$G_{11}=c_{0,0}\cdot\left(n_0\right)^2+c_{5,5}\cdot\left(n_1\right)^2+c_{4,4}\cdot\left(n_2\right)^2+2\cdot c_{0,5}\cdot n_0\cdot n_1+2\cdot c_{0,4}\cdot n_0\cdot n_2+2\cdot c_{4,5}\cdot n_1\cdot n_2$$

$$G_{12}=c_{0,5}\cdot\left(n_0\right)^2+c_{1,5}\cdot\left(n_1\right)^2+c_{3,4}\cdot\left(n_2\right)^2+\left(c_{0,1}+c_{5,5}\right)\cdot n_0\cdot n_1+\left(c_{0,3}+c_{4,5}\right)\cdot n_0\cdot n_2+$$
$$+\left(c_{3,5}+c_{1,4}\right)\cdot n_1\cdot n_2$$

$$G_{13}=c_{0,4}\cdot\left(n_0\right)^2+c_{3,5}\cdot\left(n_1\right)^2+c_{2,4}\cdot\left(n_2\right)^2+\left(c_{0,3}+c_{4,5}\right)\cdot n_0\cdot n_1+\left(c_{0,2}+c_{4,4}\right)\cdot n_0\cdot n_2+$$
$$+\left(c_{2,5}+c_{3,4}\right)\cdot n_1\cdot n_2$$

$$G_{22}=c_{5,5}\cdot\left(n_0\right)^2+c_{1,1}\cdot\left(n_1\right)^2+c_{3,3}\cdot\left(n_2\right)^2+2\cdot c_{0,5}\cdot n_0\cdot n_1+2\cdot c_{3,5}\cdot n_0\cdot n_2+2\cdot c_{1,3}\cdot n_1\cdot n_2$$

$$G_{23}=c_{4,5}\cdot\left(n_0\right)^2+c_{1,3}\cdot\left(n_1\right)^2+c_{2,3}\cdot\left(n_2\right)^2+\left(c_{3,5}+c_{1,4}\right)\cdot n_0\cdot n_1+\left(c_{2,5}+c_{3,4}\right)\cdot n_0\cdot n_2+$$
$$+\left(c_{1,2}+c_{3,3}\right)\cdot n_1\cdot n_2$$

$$G_{33}=c_{4,4}\cdot\left(n_0\right)^2+c_{3,3}\cdot\left(n_1\right)^2+c_{2,2}\cdot\left(n_2\right)^2+2\cdot c_{3,4}\cdot n_0\cdot n_1+2\cdot c_{2,4}\cdot n_0\cdot n_2+2\cdot c_{2,3}\cdot n_1\cdot n_2$$

Fig. 4-4 Expression of the Christoffel matrix ***G*.**

$$G=\begin{pmatrix}G_{11} & G_{12} & G_{13}\\ G_{12} & G_{22} & G_{23}\\ G_{13} & G_{23} & G_{33}\end{pmatrix}$$

Christoffel matrix for piezoelectric solid:

$$\varepsilon 1\cdot n\cdot n=\varepsilon_{11}$$

$$GG=G+\frac{\gamma\cdot\gamma^T}{\varepsilon 1\cdot n\cdot n}$$

$$GG=\begin{pmatrix}c_{11} & 0 & 0\\ 0 & \frac{c_{11}-c_{12}}{2} & 0\\ 0 & 0 & c_{44}+d_{15}^2\cdot\frac{c_{44}^2}{\varepsilon_{11}}\end{pmatrix}$$

Fig. 4-5 Expression of the Christoffel matrix ***G*** for piezoelectric solid.

Solution for non-piezoelectric solid:

$$\text{eigenvals}(G)=\begin{pmatrix} c_{11} \\ \frac{c_{11}-c_{12}}{2} \\ c_{44} \end{pmatrix}$$

$$\text{eigenvecs}(G)=\begin{pmatrix} 1 & 0 & 0 \\ 0 & 1 & 0 \\ 0 & 0 & 1 \end{pmatrix}$$

Solution for piezoelectric solid:

$$\rho \cdot v^2=\text{eigenvals}(GG)$$

$$\rho \cdot v^2=\begin{pmatrix} c_{11} \\ \frac{c_{11}-c_{12}}{2} \\ c_{44} \cdot \frac{\varepsilon_{11}+d_{15}^2 \cdot c_{44}}{\varepsilon_{11}} \end{pmatrix}$$

$$GG\begin{pmatrix} 1 \\ 0 \\ 0 \end{pmatrix}=\begin{pmatrix} c_{11} \\ 0 \\ 0 \end{pmatrix} \qquad GG\begin{pmatrix} 0 \\ 1 \\ 0 \end{pmatrix}=\begin{pmatrix} 0 \\ \frac{c_{11}-c_{12}}{2} \\ 0 \end{pmatrix} \qquad GG\begin{pmatrix} 0 \\ 0 \\ 1 \end{pmatrix}=\begin{pmatrix} 0 \\ 0 \\ c_{44}+\frac{d_{15}^2 \cdot c_{44}^2}{\varepsilon_{11}} \end{pmatrix}$$

Fig. 4-6 The relationship between ultrasonic velocity and elastic constants.

4.2 Poled PZT ceramic samples

PZT ceramic samples of type APC856 (soft), APC850 (soft) and APC841 (hard) were provided by American Piezoceramics International, Mackeyville, PA, USA. There were used the next types of samples of PZT ceramics:

1) Disc shaped samples of type APC841, APC850 were 10 mm in diameter, 1 mm in thickness. The samples were polarized in direction of their thickness and measured in the same [001] direction.

2) Rectangular plate samples of type APC841, APC850, APC856 with dimension $7\times14\times1$ mm^3 were polarized along their thickness or length directions. Samples were measured in [100] direction and/or in [001] direction. Both unpoled and by manufacturer polarized samples were measured. Fig. 4-7 shows types of measured samples placed in coordinate axes system. Electrode pattern, directions of polarization and wave propagation are shown.

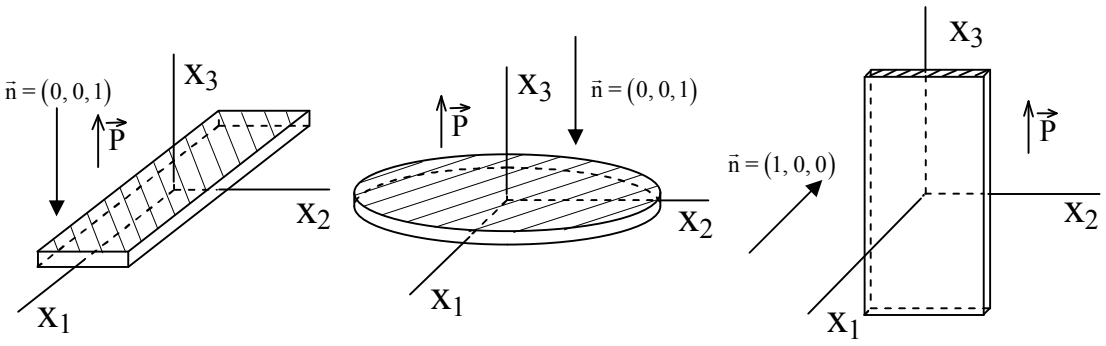

a) Propagation direction [100] b) Propagation direction [100]

Fig. 4-7 Measured samples placed in coordinates axes system.

The poled PZT type ceramics exhibit the averaged crystal symmetry ∞mm. Typically, the poling direction of ceramic samples is [001] direction.

The result of study of the influence bias electric field on velocity of the propagation of longitudinal and transverse ultrasonic waves in PZT ceramic samples were presented at the conference POLECER in Liberec, 2007 and published in [31].

The relationships between the measured ultrasonic phase velocities and related elastic constants were derived from the Christoffel wave equations for various directions of ultrasonic wave propagation, and these relationships have been expressed using MathCAD v.13.0

The relations between the linear elastic coefficient c_{44}^{E} and the velocity of shear waves propagating along the [001] direction can be expressed as:

$$c_{44}^{E} = \rho\left(v_{\text{shear}[010],[100]}^{[001]}\right)^2 \tag{15}$$

The relations between the velocity of longitudinal waves propagating along the [100] direction and the linear elastic coefficient c_{11}^{E} were expressed as:

$$c_{11}^{E} = \rho\left(v_{\text{long}}^{[100]}\right)^2 \tag{16}$$

Electrically clamped conditions are supposed for the high fundamental frequencies of used transducers, which are operating at 15 and 22 MHz.

The samples were protected in oil bath from sparking on edges of samples. Thin aluminum foil was used as removable electrodes. The good electric conductivity and ultrasonic coupling were realized by suitable coupling material. A honey was used as a very good material for shear wave coupling at frequencies 10-20 MHz at room temperature.

We can observe the poling process on virgin sample in electric field, on Figs. 4-8 and 4-9.

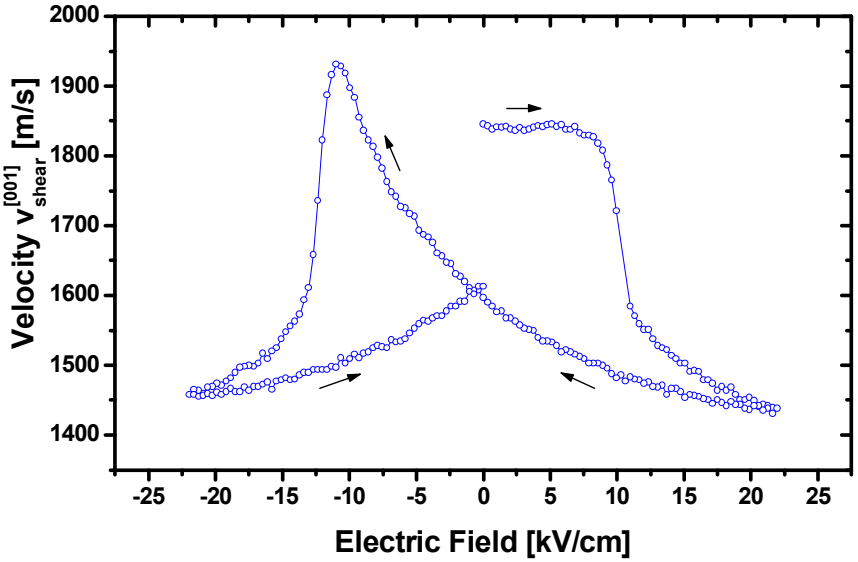

Fig. 4-8 Shear mode velocity $v_{\text{shear}[100],[010]}^{[001]}$ as a hysteresis dependence of electric field on unpoled sample of PZT ceramics APC 850, disc 10 mm in diameter, 1 mm in thickness.

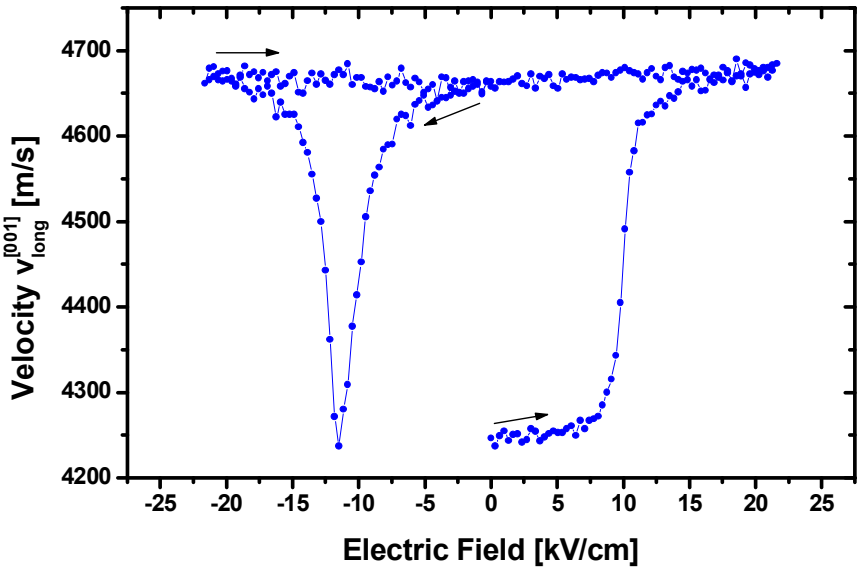

Fig. 4-9 Longitudinal mode velocity $v_{\text{long}}^{[001]}$ as a function of electric field on unpoled sample of PZT ceramics APC 850, disc 10 mm in diameter, 1 mm in thickness.

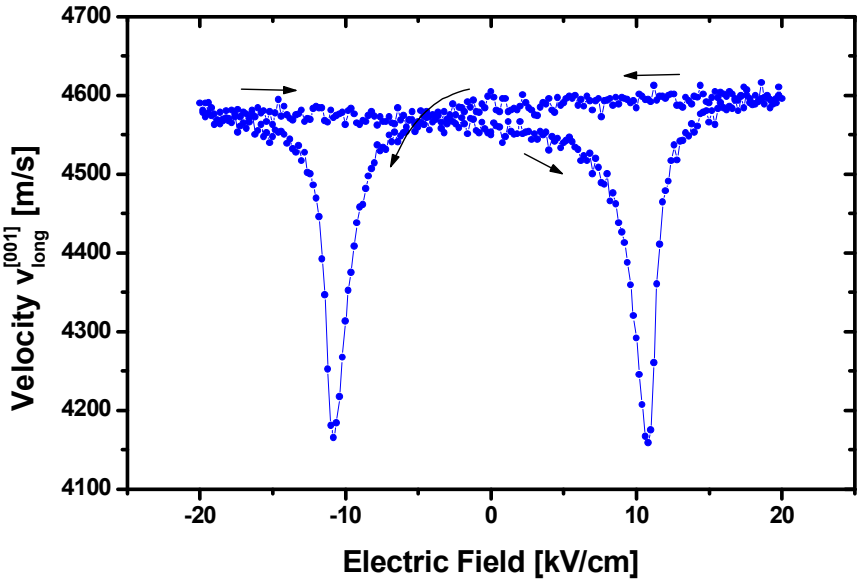

Fig. 4-10 Longitudinal mode velocity $v_{long}^{[001]}$ as a function of electric field for poled sample of PZT ceramics APC 850.

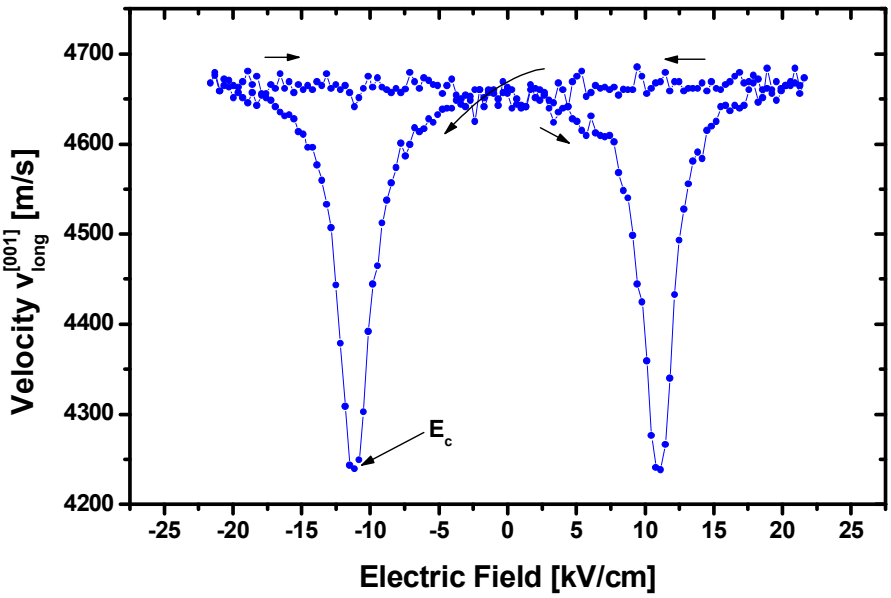

Fig. 4-11 Longitudinal mode velocity $v_{long}^{[001]}$ as a function of electric field for the sample of PZT ceramics APC 850, disc 10 mm in diameter, 1 mm in thickness. Sample was not polarized.

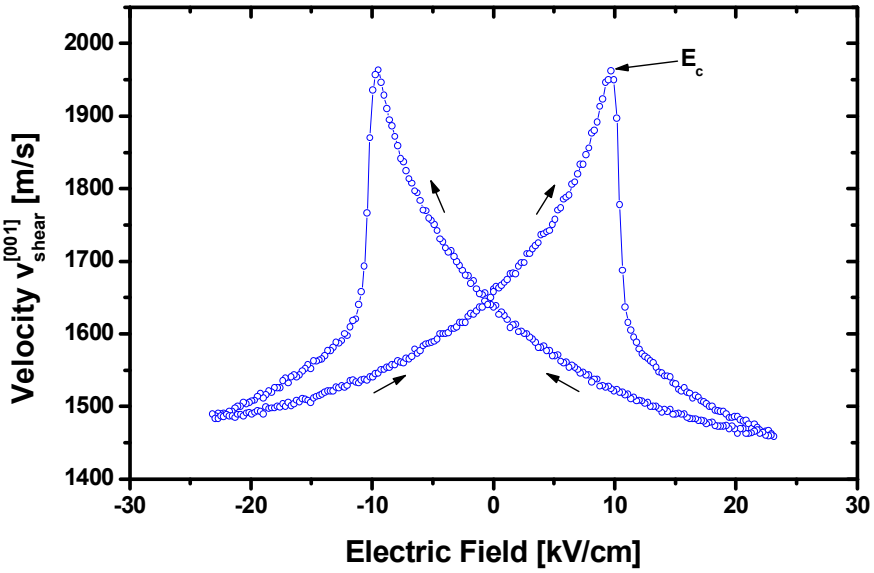

Fig. 4-12 Shear mode velocity $v^{[001]}_{shear[100],[010]}$ as a function of electric field for poled sample of PZT ceramic APC 850, disc 10 mm in diameter, 1 mm in thickness.

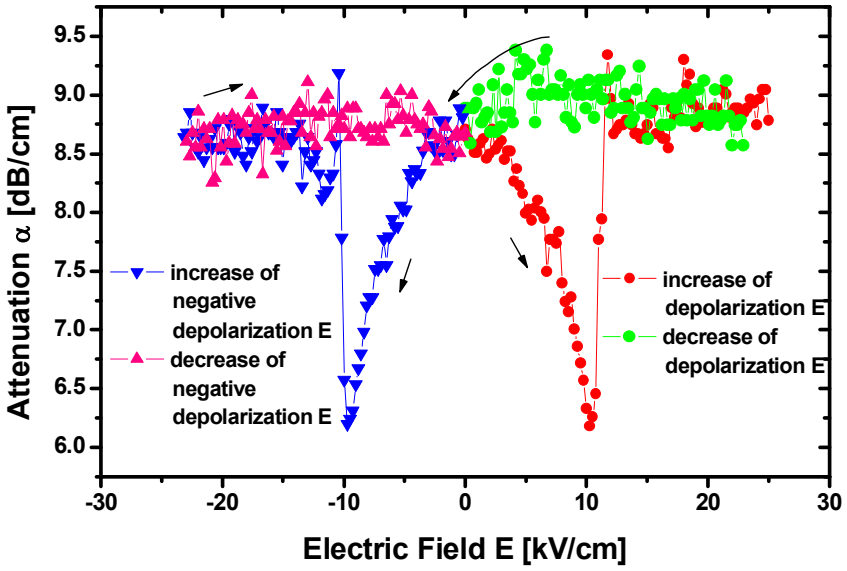

Fig. 4-13 Attenuation of shear wave as a function of electric field on poled sample of PZT ceramic APC 850, disc 10 mm in diameter, 1 mm in thickness.

Figs. 4-10, 4-11 and 4-12 show hysteresis loops of ultrasonic velocity versus bias electric field. The measurements were realized in a special sample holder connected to Matec ultrasound system controlled by computer. At the beginning of the measurements, the electric field was applied in the direction opposing the sample polarization. When the field was gradually increased, the longitudinal velocity was almost unchanged until the electric field magnitude reaches approximately 13 kV/cm for both positive and negative field directions. The velocity begins to decrease quickly with increasing field when above the critical points. The velocity reaches a minimum in the vicinity of the coercive field E_c and then drastically increases back to its original value, if the field level increases (Figs. 4-10, 4-11).

For shear waves, the velocities start to increase with increasing electric field and reach maxima near the coercive field E_c. Above these critical points, the velocity falls down with increasing electric field and reaches a minimum. With electric field decreasing, the velocity increases to the original value (Fig. 4-12). Asymmetrical hysteresis loop for hard ceramics were observed, which is due to the domain pinning effect by the oxygen vacancies in hard materials.

The change of acoustic attenuation during polarization for shear mode ultrasound wave is shown in the Fig. 4-13.

PZT ceramics is in ferroelectric phase with various possible domain states at room temperature. The dipole of each unit cell can be formed along the allowed directions. During application of the electric field, some orientations of polarization become energetically preferable. Direction of polarization follows external electric field.

From Equation 15, the relation between the velocity of shear waves propagating along the [001] direction and the linear elastic coefficient c_{44}^{E} for [001] poled sample is:

$$v_{\text{shear}[010],[100]}^{[001]} = \sqrt{\frac{c_{44}^{E}}{\rho}} \tag{17}$$

During repolarization process, by applying the reverse electric field, the polarization directions jump to energetically preferable states. Its leads to the increment

of perpendicular component of polarization and piezoelectric contribution to the propagation of transversal mode of ultrasonic waves (see Equations 18, 19):

$$v_{\text{shear}[001]}^{[100]} = \sqrt{\frac{d_{15}^2 \cdot \left(c_{44}^E\right)^2 + c_{44}^E \cdot \varepsilon_{11}^S}{\rho \cdot \varepsilon_{11}^S}} \tag{18}$$

$$v_{\text{shear}[010]}^{[100]} = \sqrt{\frac{c_{11}^E - c_{12}^E}{\rho}} \tag{19}$$

where $c_{\lambda\mu}^E$ and $d_{i\lambda}$ denote the elastic stiffness constants under constant electric field and piezoelectric charge constants in matrix notation, respectively.

The situation is found to be opposite for the case of longitudinal waves. The relationship between the velocity of longitudinal waves propagating along the [001] direction (including contribution of the piezoelectric effect), and the linear elastic coefficients c_{33}^E and c_{13}^E for [001] poled sample is:

$$v_{\text{long}}^{[001]} = \sqrt{\frac{\left(c_{13}^E \cdot 2d_{31} + d_{33} \cdot c_{33}^E\right)^2 + c_{13}^E \cdot \varepsilon_{33}^S}{\varepsilon_{33}^S \rho}} \tag{20}$$

With increasing perpendicular component of polarization, the piezoelectric contribution to the propagation of longitudinal mode of ultrasonic waves is found to decrease (see Equation 21).

$$v_{\text{long}}^{[100]} = \sqrt{\frac{c_{11}^E}{\rho}} \tag{21}$$

The sound velocity was found to change drastically near the coercive field for a PZT ceramics. The velocity of longitudinal waves decreases with an increasing field while the velocity of shear waves increases, which is caused by the change of the elastic anisotropy under influence of the depolarization field. The consequent change of the piezoelectric contribution to effective elastic constant decreases the velocity of longitudinal waves and at the same time increases the velocity of shears waves around the coercive field.

In Table 1 are collected velocity measurements and some elastic constants, calculated from the measurements of the velocities of longitudinal and shear waves in absence of applied electric field for poled samples at room temperature. The results show that the elastic moduli c_{11}^{E} of the hard ceramics APC 841 are approximately 15 % higher then the elastic moduli of the soft ceramics (APC 850, APC 856).

Table 1. Some elastic constants and measured velocities for longitudinal and shear waves in samples polarized in [100] (marked with *) and [001] directions.

Sample	Velocity [m/s]					Elastic moduli [10^9 Pa]	
	$v_{\text{long}}^{[100]}$	$v_{\text{long}}^{[001]}$	$v_{\text{shear}[001]}^{[100]}$	$v_{\text{shear}[010]}^{[100]}$	$v_{\text{shear}[010],[100]}^{[001]}$	c_{11}^{E}	c_{44}^{E}
APC 841*	4423		2542	2148		148.7±1.4	
APC 841		4690			1857		26.2±0.3
APC 850		4565			1651		21.0±0.1
APC 850*	4145		2302	1797		132.3±0.8	
APC 856*	4130		2247	1870		127.9±0.4	

4.3 Poled PZN-PT samples

Crystal cuts [001], [110] and [111] served for measurements of the elastic stiffness constants under application of the electric field. The result of study of the influence bias

electric field on velocity of the propagation of longitudinal and transverse ultrasonic waves in PZN-PT crystals were presented at the conference ECAPD'7 in Liberec, 2004 and published in [32]. The elastic coefficients of PZN-PT crystals at room temperature for various frequencies of ultrasonic transducer were calculated. Fig. 4-14 shows longitudinal mode velocity and attenuation of the ultrasonic wave, as functions of electric field for [110] direction in PZN-4.5%PT sample.

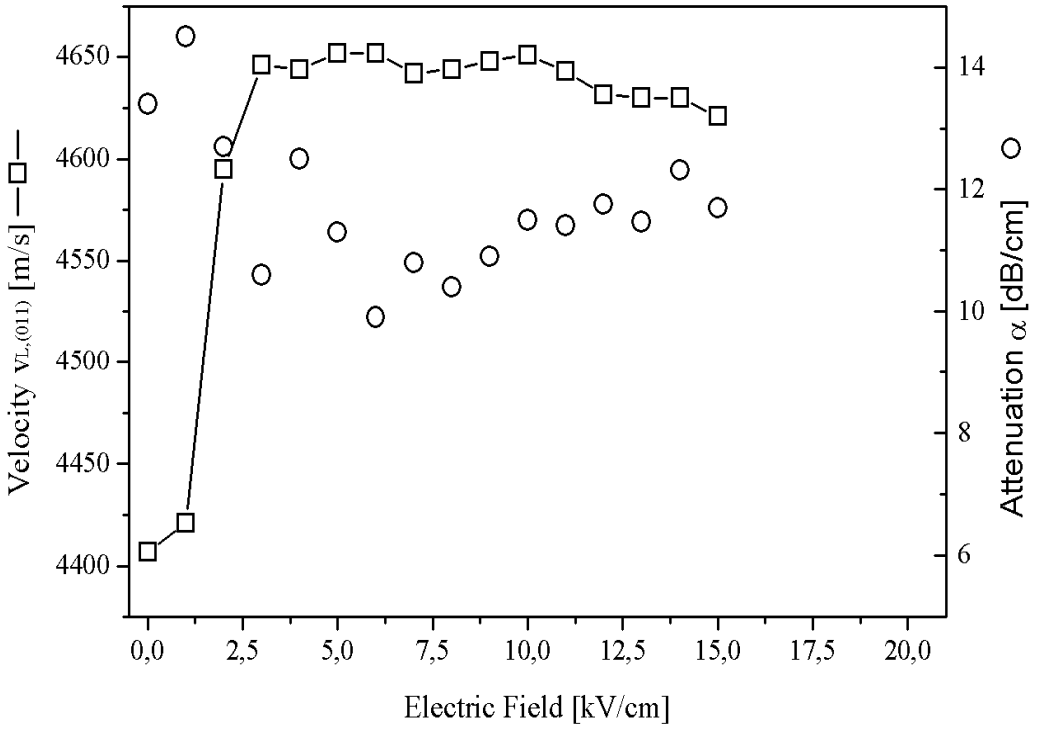

Fig. 4-14 The longitudinal mode velocity and attenuation as functions of the electric field for [110] direction in PZN-4.5%PT sample.

Measurements were realized on Matec model 7700. From these measurements, the values of complex elastic stiffness constants are evaluated at different poling conditions with different frequencies for longitudinal and shear excitations. The purpose of this work was to characterize electric field induced phase transitions of PZN-4.5%PT single crystals cuts at room temperature and influence of the electric bias field on the elastic stiffness constants. There are three used crystal orientations. The first one is [001],

[010] and [100], the second one is [110], $[1\bar{1}0]$ and [001] and the third one is [111], $[1\bar{1}0]$ and $[11\bar{2}]$. The dimensions of all samples are 4 x 4 x 2 mm^3. The axis normal to the largest plain is the x_1 axis.

The relations between the velocity and the linear elastic coefficient c_{33}^E, for a system poled at [001] direction with waves propagating along the [001] direction, with contribution of piezoelectric effect can be expressed:

$$\rho v_{\text{long}[001]}^2 = c_{33}^E + \frac{e_{33}^2}{\varepsilon_{33}} = c_{33}^E + \frac{4}{\varepsilon_{33}}\left(\left(d_{31}c_{13}^E\right)^2 + d_{31}d_{33}c_{13}^E c_{33}^E + \frac{\left(d_{33}^E c_{33}^E\right)^2}{4} \right) \tag{22}$$

Where $c_{\lambda\mu}^E$, $e_{i\lambda}$ and $d_{i\lambda}$ are the elastic stiffness constants with constant electric field, piezoelectric strain coefficients and piezoelectric constants in matrix notation.

For waves propagating along the [110] direction the following relations between the velocities and the linear elastic coefficients c_{11}, c_{12} and c_{44}:

$$\rho v_{\text{long}[110]}^2 = \rho v_{\text{long}[1\bar{1}0]}^2 = \left(c_{11} + c_{12} + 2c_{44}\right)/2 \tag{23}$$

The phase velocity of the shear wave that propagates along [110] and is polarized in $[\bar{1}10]$ direction is related to elastic stiffness constant by the relation:

$$\rho v_{\text{shear}[110]}^2 = \left(c_{11} - c_{12}\right)/2 \tag{24}$$

Electrically clamped conditions are supposed for the high fundamental frequencies of used transducers, which are operating at 15 and 22 MHz.

4.4 Temperature and electric field bias measurements

The velocities of longitudinal ultrasonic waves in Lead Zinc Niobate-Lead Titanate (PZN-PT) single crystal samples in various crystal orientations were investigated as a function of temperature. The influence of an electric DC bias field on the elastic stiffness at various temperatures in vicinity of a phase transition is studied. The results were presented at the conference POLECER 2007 in Liberec, and published in [33].

The experiments are realized inside a special temperature chamber working in temperature range from -50 °C up to 200 °C with the option for DC bias fields and with an absolute accuracy ±0.1 °C. The bias field was applied by a high voltage amplifier Trek model 610D. The thin layer of honey was put on the ultrasonic transducer, then aluminum foil, which served as an electrode, and then again a thin layer of honey and the measured sample was put.

Fig. 4-15 shows the temperature chamber for electric field dependence ultrasonic measurement.

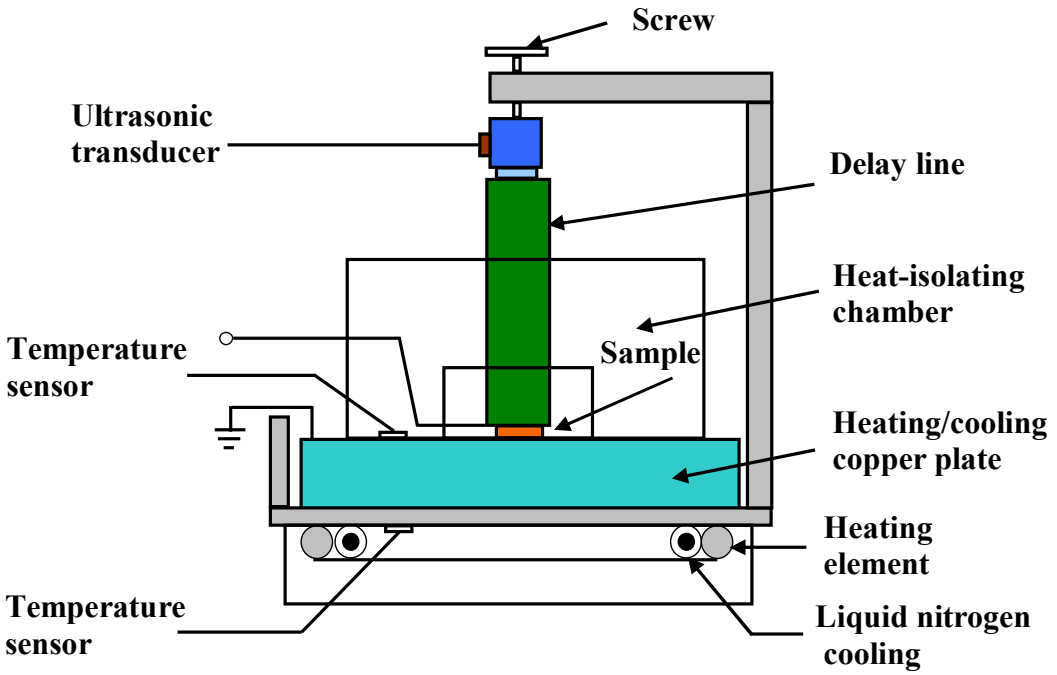

Fig. 4-15 Temperature chamber for electric field dependence ultrasonic measurement.

The program for automatic recording of measured ultrasonic response from an oscilloscope has been developed in HP Vee program. Search of the time of flight of ultrasound waves through the sample was made simultaneously by three methods. First: by measuring the time distance between two maxima of a response, second: by evaluation of the average value of the time distance between all subsequent maxima of the measured response, third: in a manual mode by visual adjustment of cursors of oscilloscope on peaks of an ultrasonic response, with the subsequent calculation of time distance between cursors. An automatic measurement does not always cope to record the maximum of a response in the vicinity of some phase transitions, therefore the simultaneous correction of time of flight measurements by means of manual measurement of time of flight was made. The adjustment (tuning) of resonance frequency of the ultrasonic transducer was made before each measurement, because of dependence of the quality of an ultrasonic response on the attenuation, the type and a way of polarization of the sample and the type of ultrasonic wave polarization.

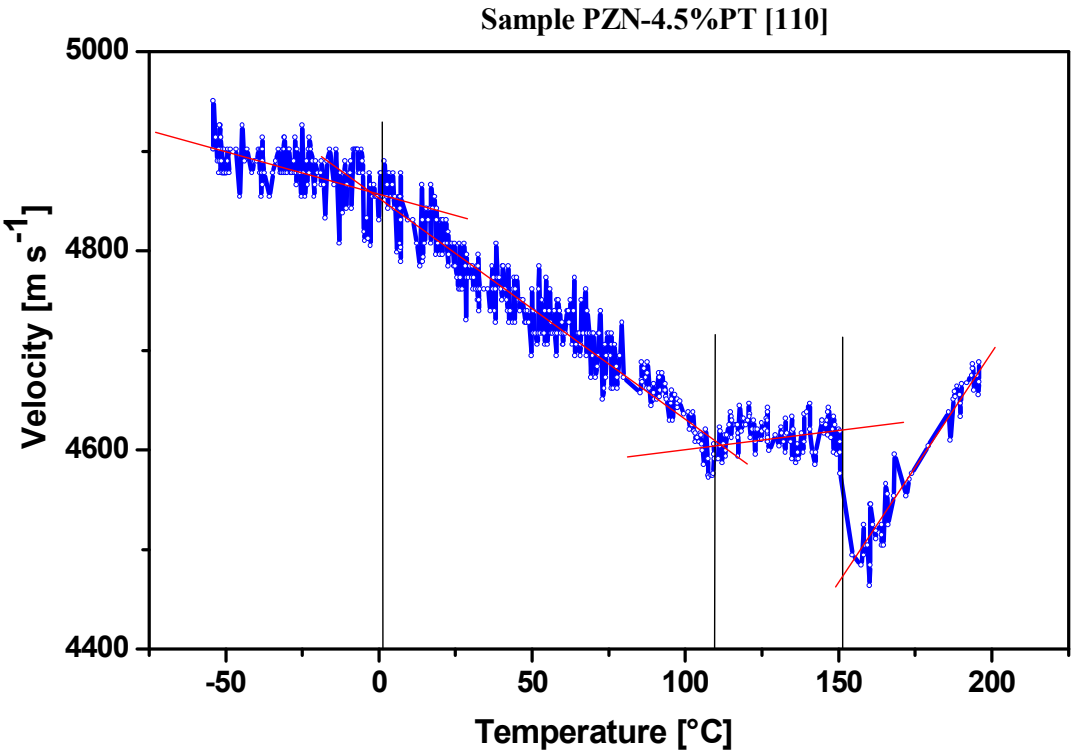

Fig. 4-16 Temperature dependence of longitudinal wave velocity of the [110] cut.

Temperature dependence of ultrasound velocity of PZN-PT crystal samples were measured in temperature range -30 °C up to 180 °C. The rate of heating was 1 °C /min.

In Figs. 4-16 and 4-17 we can see different behavior of longitudinal ultrasound waves propagating in two different directions. Structural ferroelectric phase transitions from the rhombohedral to the tetragonal symmetry are well visible on both figures at a temperature of approximately 120 °C. A paraelectric phase transition is observed at about 150 °C.

Fig. 4-17 shows a process of polarization rotation through monoclinic phases into a tetragonal state. The various behavior of ultrasound longitudinal wave propagation is simply given by the direction of propagation with regard to the polarization direction.

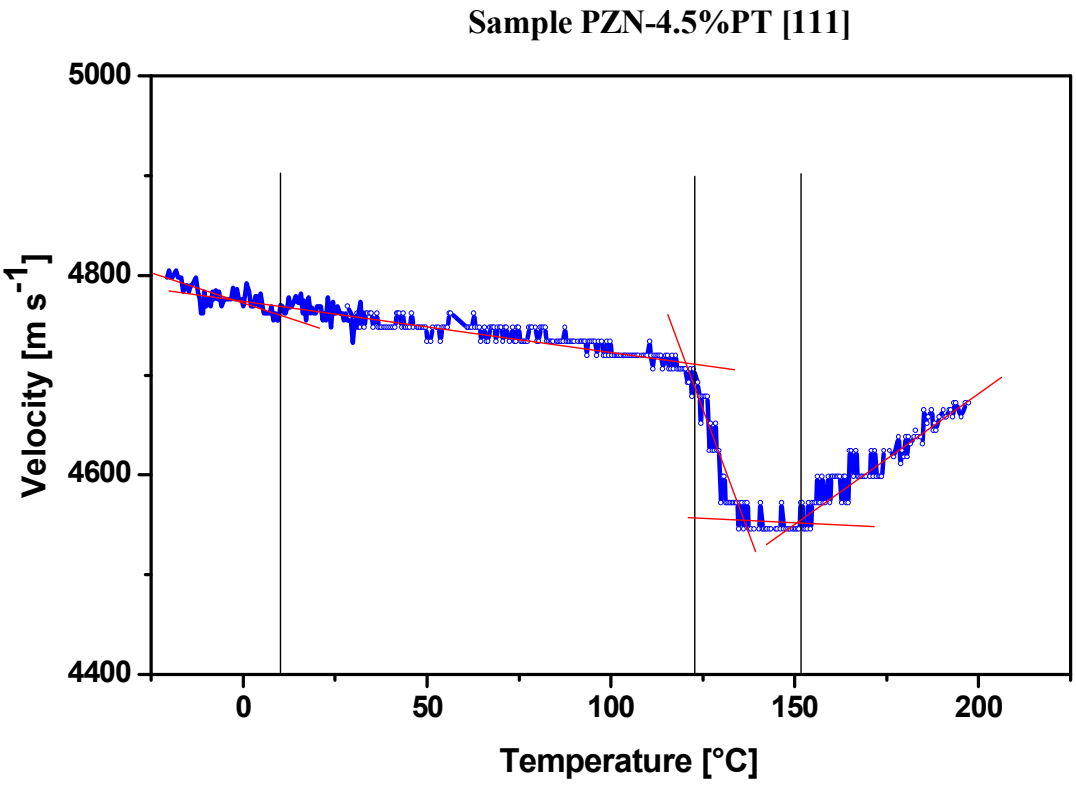

Fig. 4-17 Temperature dependence of longitudinal wave velocity of the [111] cut.

Fig. 4-17 illustrates the measurement of the longitudinal wave velocity for a sample cut along the [111] direction under equivalent conditions. We can observe the same regions as for a cut along the [110] direction. The temperature of the sample is set

by direct contact with copper thick plate heated resistively and a cooling pipe on the bottom with an exhaust of nitrogen vapors on the sample. The metal plate serves as the ground electrode, too. Electric field measurements were realized in the same sample holder. A thin aluminum foil is placed between the sample and the quartz delay line providing good electric and acoustic contact. The slot around the sample is filled by silicon oil to prevent breakdown on the outside edges of the sample.

Crystal cuts of [001], [110] and [111] were used for the study of electric field poling conditions and temperature influence on structure induced by polarization orientation. PZN-PT samples of the composition 4.5 % and 8 % with thickness 0.5 mm and width 4 x 4 mm^2 were prepared. Samples, poled during measurements, were depoled by annealing at temperature above Curie temperature T_c and again measured.

Fig. 4-18 shows the structure of the cubic, tetragonal, rhombohedral and orthorhombic phases. Miller indices are used to define the orientation of the crystals. A transformation from the cubic to the tetragonal, rhombohedral or orthorhombic phases results in a spontaneous polarization in a [001], [111] or [110] direction respectively.

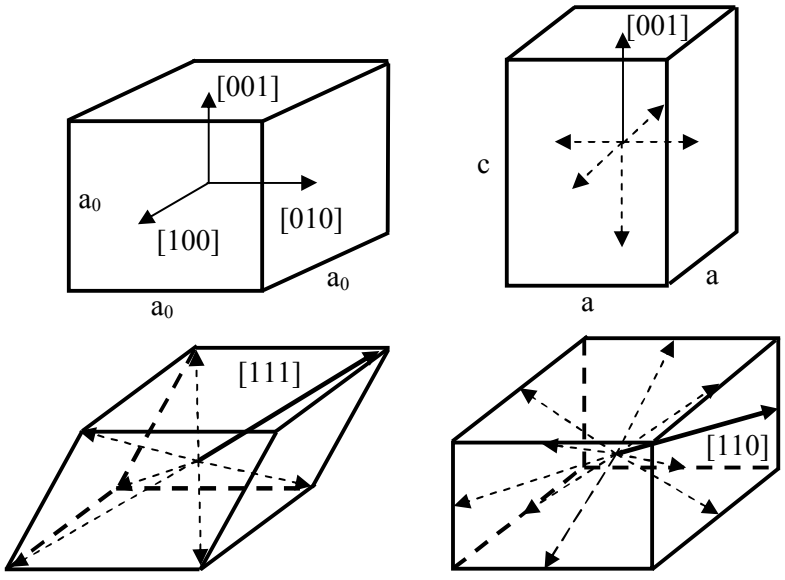

Fig. 4-18 PZN-PT single crystal: phases and crystal equivalent polarization directions.

As shown in Fig. 4-18, the tetragonal phase has 6 equivalent polarization directions, the rhombohedral phase has 8, and the orthorhombic phase has 12 ones. Local coordinates are used for each crystal variant with the X_3 direction parallel to the spontaneous polarization. For a [001] direction cut of tetragonal phase, X_1-X_2-X_3 lie along the [100]-[010]-[001] directions; for a [111] cut orientation of rhombohedral phase, X_1-X_2-X_3 lie along the $[1\bar{1}0]$-$[11\bar{2}]$-[111] directions; for a [110] cut orientation of orthorhombic phase, X_1-X_2-X_3 lie along the [001]-$[1\bar{1}0]$-[110] directions, see Figs. 4-19, 4-20 and 4-21.

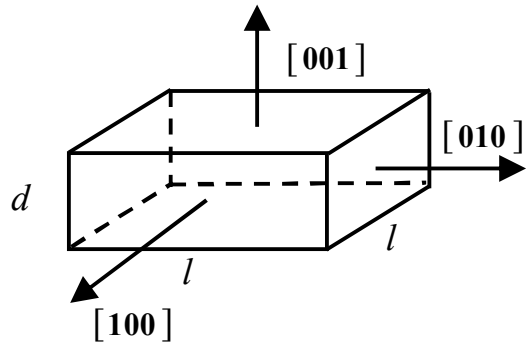

Fig. 4-19 Sample of [001] cut orientation.

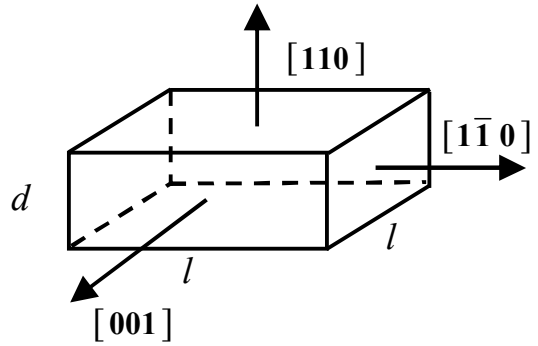

Fig. 4-20 Sample of [110] cut orientation.

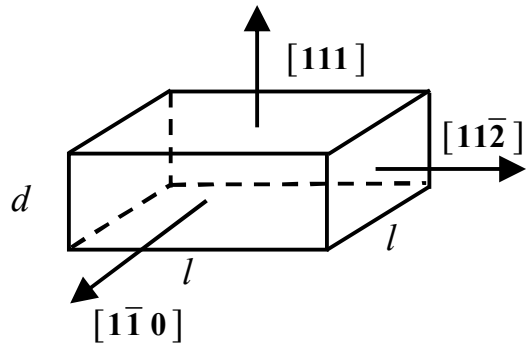

Fig. 4-21 Sample of [111] cut orientation.

During increasing temperature, we can observe the change of ultrasound velocity, regions in the temperature range with various tangents of linear dependence, which means that crystal has a phase transitions. The strong influence of relatively small electric field on ultrasound phase velocity was observed.

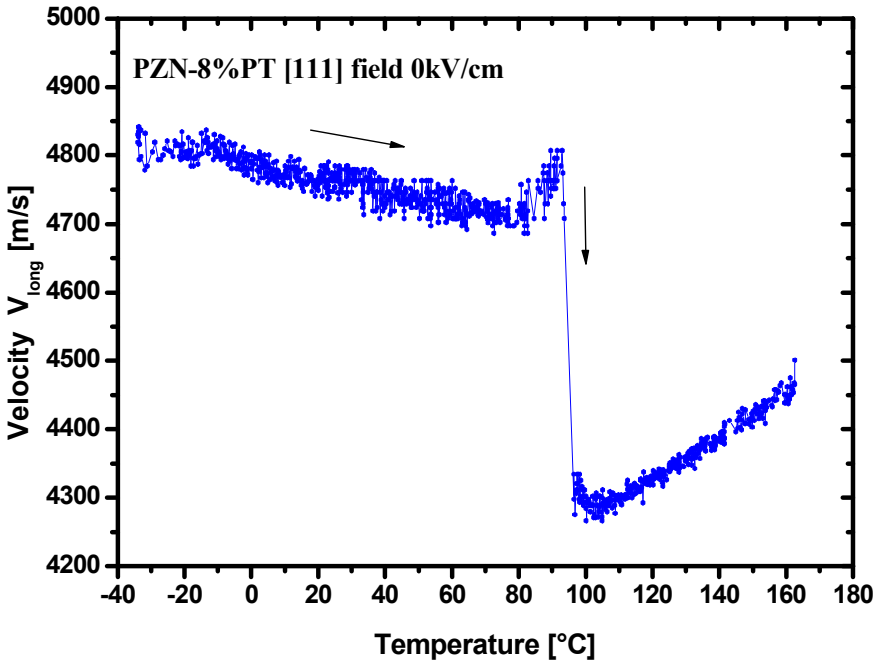

Fig. 4-22 Longitudinal mode velocity $v_{long}^{[111]}$ as a function of temperature on PZN-8%PT [111] sample**.**

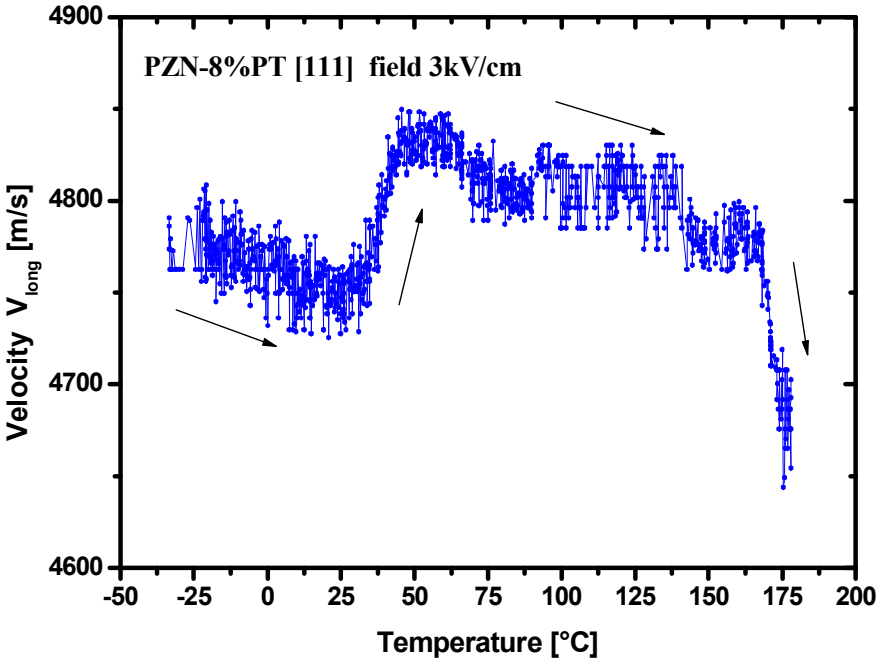

Fig. 4-23 Longitudinal mode velocity $v_{long}^{[111]}$ as a function of temperature on PZN-8%PT [111] sample under DC field 3 kV/cm.

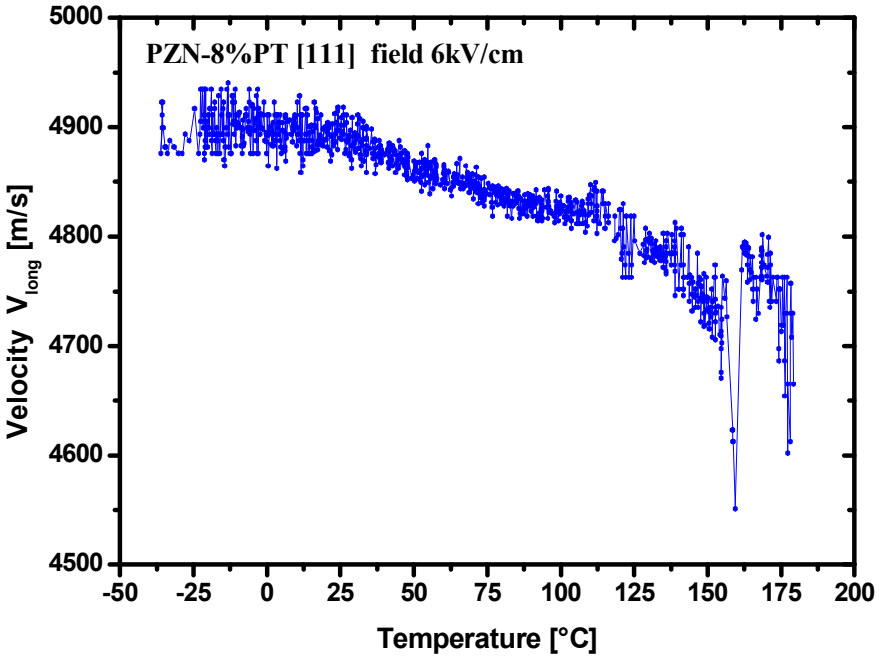

Fig. 4-24 Longitudinal mode velocity $v_{long}^{[111]}$ as a function of temperature on PZN-8%PT [111] under DC field 6 kV/cm.

Figs. 4-22, 4-23 and 4-24 show the temperature dependence of longitudinal mode velocity $v_{long}^{[111]}$ under various electric fields. The measurement of dependencies of ultrasound wave velocities on temperature became complicated at temperatures substantially higher that the room ones because of crystallization of the honey, and damage of ultrasonic contact between the transducer and the measured sample.

On Fig. 4-25 we can observe the process of poling of virgin sample by electric field applied in [111] direction. The increasing of sound velocity of poled sample compared to unpoled ones is a result of the piezoelectric contribution to the elastic constants. We can observe electric field induced phase transition.

The domain engineered samples PZN-4.5%PT cut [001] and PZN-8%PT cut [111] exhibit at low electric fields stepwise change in speed of ultrasound, see Figs. 4-26, 4-27 and 4-28. This is caused by domain reorientation and the consequent stabilization of domain structure.

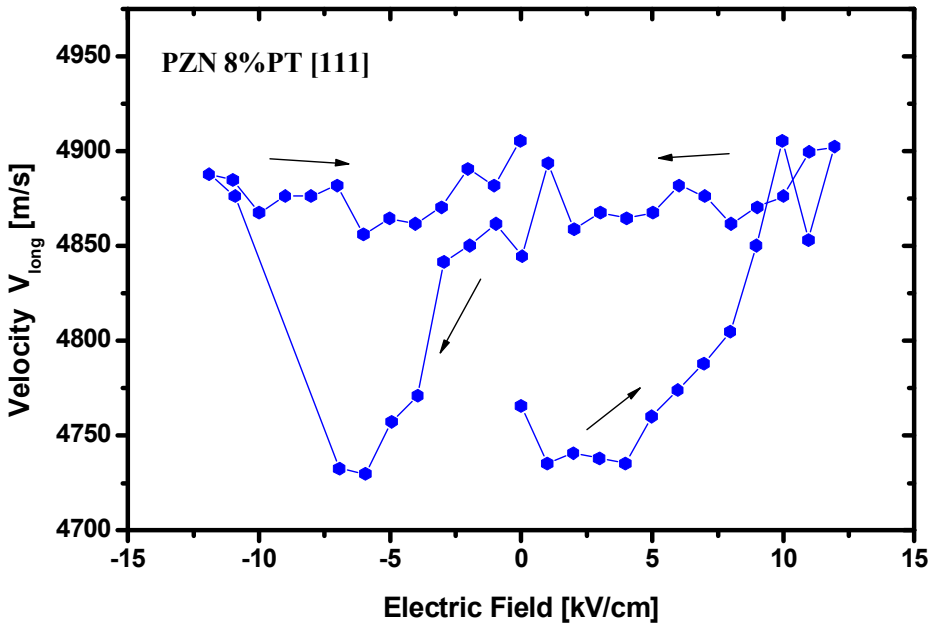

Fig. 4-25 Longitudinal mode velocity $v_{long}^{[111]}$ as a function of electric field on unpoled PZN-8%PT [111] sample at room temperature.

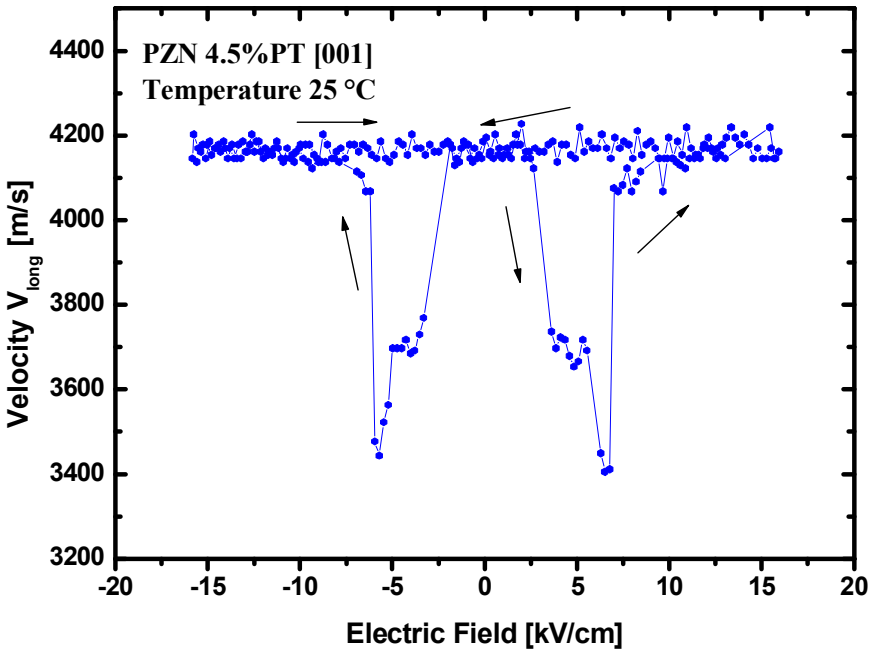

Fig. 4-26 Longitudinal mode velocity $v_{long}^{[001]}$ as a function of electric field on PZN-4.5%PT [001] sample at room temperature.

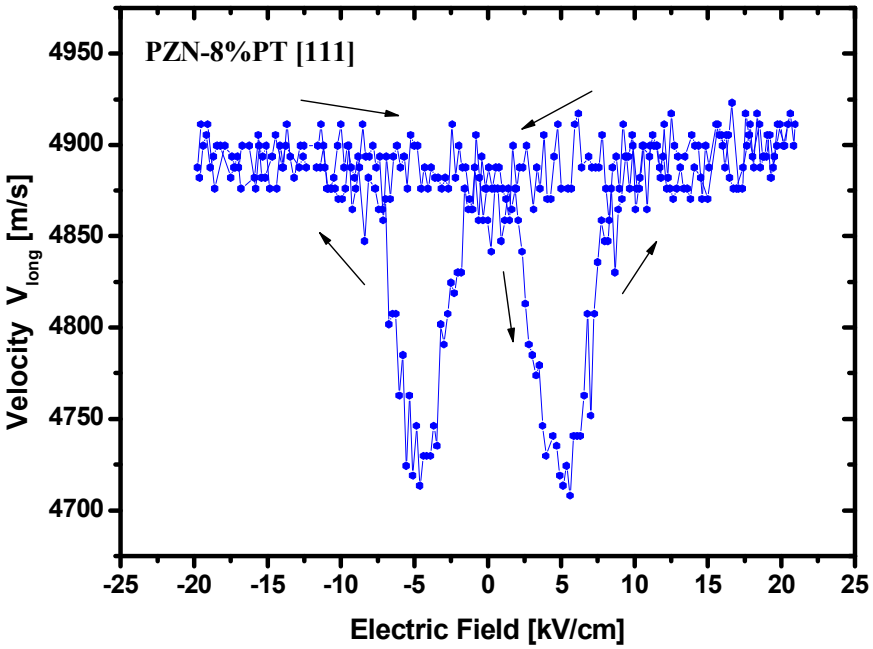

Fig. 4-27 Longitudinal mode velocity $v_{long}^{[111]}$ as a function of electric field on PZN-8%PT [111] sample at room temperature.

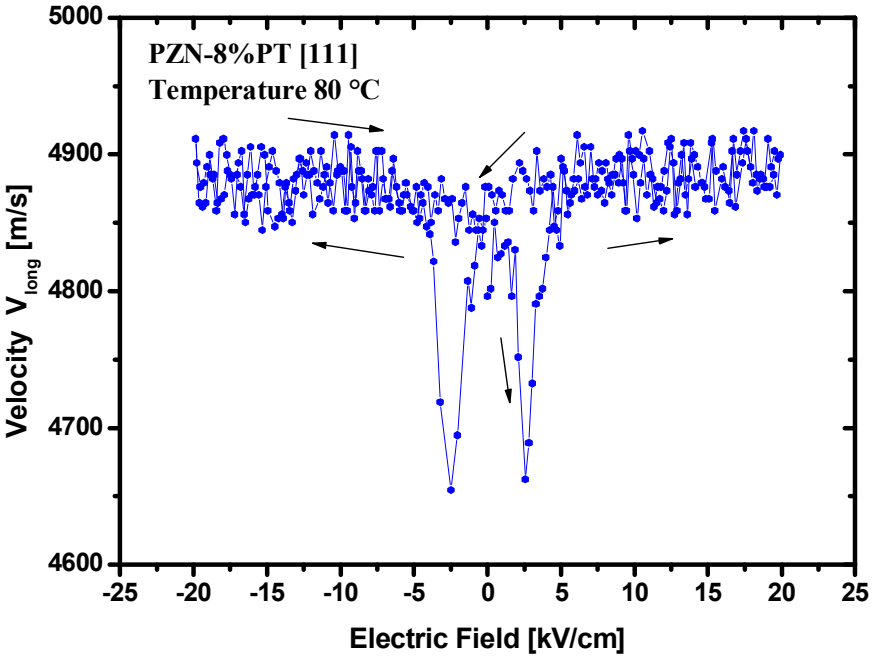

Fig. 4-28 Longitudinal mode velocity $v_{long}^{[111]}$ as a function of electric field on PZN-8%PT [111] sample at 80 °C.

Fig. 4-29 shows a hysteresis loops of longitudinal ultrasonic phase velocity versus electric field at various temperatures. For a comparison, a hysteresis loops obtained at various temperatures are shown at the same figure. The electric field was applied to the sample along the [001] direction, and the phase velocity of ultrasound in [001] direction was measured. The electric field was applied opposing the polarization at the beginning. The behavior of hysteresis loops for PZN-PT crystals and PZT ceramics is analogous. The velocity reaches a minimum near the coercive field E_c and then drastically increases back to its original value with further increase of the field level. These results are in a good agreement with [22].

Some measurements for some crystals cuts were almost impossible with our equipment because of disappearance of a response at heating the sample to 50 degrees and above. That could be result of the increase of the attenuation for the given orientation of crystal. The shape of the hysteresis loops for electric field measurements changed with the increasing temperature, so that the coercive field decreased. We can see different behavior of the velocity of ultrasound wave propagation with increasing

temperature for various cuts of single crystals. The various phase velocity changes during phase transitions may be caused by various crystallographic phases for crystal cuts at various temperatures.

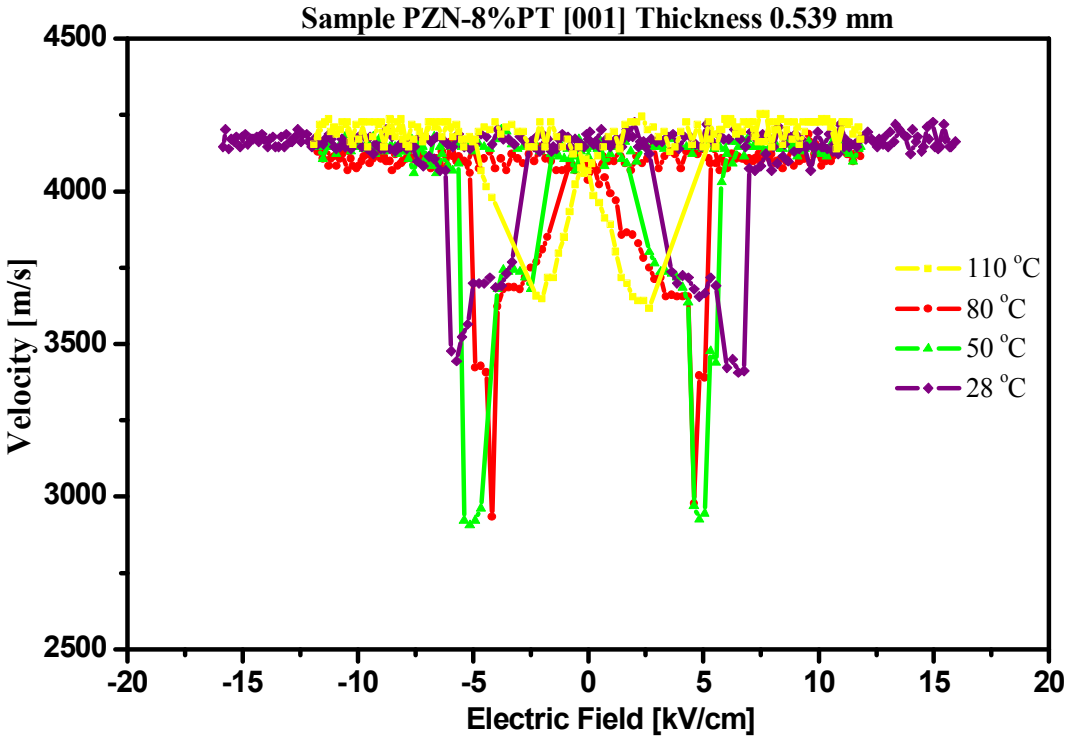

Fig. 4-29 Phase velocity of longitudinal ultrasound wave, measured at various temperatures under various electric fields. Phase velocities were measured along [001] direction and the electric field is applied along [001].

5. Discussion

The velocity and the attenuation measurements allow us to accurately study domain states and/or existence of more stable phases, and their evolution versus field and temperature. The attenuation measurement exhibits extremely high sensitivity to structure changes but the explanation of this behavior is directly connected to microscopic structure and is more complex. It is necessary to use additional experimental methods to describe this behavior.

So, the elastic anisotropy is changed under influence of the depolarization field. It leads to decrease of the velocity of longitudinal waves with an increasing electric field, while the velocity of shear waves increases. Besides, the velocity of longitudinal waves decreases around the coercive field due to the consequent change of the piezoelectric contribution to effective elastic constant, meanwhile the velocity of shear waves increases.

Different shapes of hysteresis loops for longitudinal and shear mode waves propagation are probably caused by distribution of local polarization. In case of hysteresis loop for longitudinal wave propagation, the stabilization effect of external electric field on local polarization is present. The shear wave hysteresis loop exhibits butterfly shape due to the random distribution of polarization direction in plane, perpendicular to applied electric field.

In all DC bias electric field measurements we can observe strong influence of poling direction of electric field on the process of polarization and induced phase transitions.

The evident change in phase velocity at low temperature (≈10 °C) can be attributed to the existence of a monoclinic phase mixed with a rhombohedral one. At higher temperatures we can observe a structural transition from rhombohedral to tetragonal crystal symmetry and a phase transition from the ferroelectric phase and tetragonal symmetry to the paraelectric phase represented by the parental cubic symmetry. The effect of the electric field applied to unpoled samples suggests the existence of a number of stable structures. In the case of a sample cut along [110] we induce structures with rhombohedral symmetry, two possible polarization directions, at low applied

electric fields and orthorhombic symmetry with one polarization direction for high electric field.

6. Conclusion

Ultrasonic velocities and attenuation measurements of PZT ceramics and PZN-PT single crystals have been carried out with the ultrasonic measurements under bias electric field in a wide temperature range. The longitudinal and transverse mode of sound propagation in PZN-PT single crystals containing 4.5 % PT and 8 % PT were studied. The influence of electric field, which poles the sample, is investigated by the pulse-echo sound propagation technique. The ultrasonic velocities were measured on commercial types of PZT ceramics as APC 841, APC 850, and APC 856, at room temperature and various crystal cuts [001], [110] and [111] on single crystals. The comparison of the ultrasound velocities dependence on electric bias field was made for poled/unpoled soft ceramics. The observation of electric field induced phase transitions of PZN-4.5%PT single crystals cuts at room temperature was realized. Aspects of field-induced phase transitions in PZN-4.5%PT and PZN-8%PT single crystals at room temperature are discussed.

The basic principles of measurement both of phase velocity and attenuation and derivation of effective elastic constants are described and applied to the observed results.

The velocity, measured on poled samples, was found to be higher than on unpoled ones in longitudinal mode, while the shear mode waves behaved in reversal way. The result of study of the influence bias electric field on velocity of the propagation of longitudinal and transverse ultrasonic waves in PZN-PT crystals and PZT ceramic samples were presented at the conference ECAPD'7 2004 and at the conference POLECER in Liberec, and published in [31] and [32]. The temperature and electric field dependencies of ultrasonic wave propagation and attenuation in PZN-PT single crystal in vicinity of a phase transition were presented at the conference POLECER 2007 in Liberec, and published in [33]. This research was supported by the Grant Agency of the Czech Republic GACR 202/07/1289.

The strong dependence of phase velocity and ultrasound attenuation on electric fields and different shapes of hysteresis loops for longitudinal and shear mode waves

propagation were observed. It is possible to determine a coercive field for various types of piezoelectric ceramics (soft – hard) from the form of hysteresis loops. The change of phase velocity during supposed phase transitions in unpoled and poled states of PZT is above 9 % for longitudinal and 16 % for shear mode velocity, respectively.

The experience of ultrasound measurements has shown that ultrasonic investigations demand a carefully preparation of samples and adjustment of ultrasonic equipment for carrying out of measurements, depending on the type of an ultrasonic wave, thickness and the type of the sample. There is a necessity of search of other suitable contact materials for measurements at the higher temperatures, for expansion possibilities of ultrasonic measurements of various samples, and also necessity a delay line of different length and ultrasonic transducers, working on various resonant frequencies.

For a continuation of this work, it is necessary to study the temperature and the DC bias electric field influence on the ultrasound wave velocity for the transverse and the longitudinal polarizations for other crystal cuts, like PZN-PT [110], for other percentage amounts of PT (as example: PZN-12%PT), for crystals doped with Fe. From these measurements would be possible to perform more complete calculations of the elastic and piezoelectric coefficients, and study of temperature and DC bias electric field dependencies of these coefficients.

7. References

[1] Wang H., Cao W.: Determination of full set material constants of PZT ceramics from phase velocities. *Journal of Applied Physics* **92**, 8 (2002), 4578.

[2] Sasaki Y., Ochiai T., Takeuchi Y., Hayashi S.: Determination of Elastic Stiffness and Piezoelectric e- and d-Constant of Piezoelectric Ceramic from Ultrasonic Velocity and Dielectric Constant. *Journal of Applied Physics* **34** (1995), 4122.

[3] Wang H., Jiang W. and Cao W.: Characterization of lead zirconate titanate piezoceramic using high frequency ultrasonic spectroscopy. *Journal of Applied Physics* **85,** 12 (1999), 8083.

[4] Zhang R., Jiang B., Cao W.: Influence of sample size on ultrasonic phase velocity measurements in piezoelectric ceramics. *Journal of Applied Physics* **91** Issue 12 (2002), 10194.

[5] Cheng-Kuei Jen, Chul-Jong Chung, Shapiro, G, Jean-Pierre Monchalin, Pierre Langlois, Jean F. Bussiere: Acoustic Characterization of Poling Effects in PZT Ceramics. *Journal of the American Ceramic Society* **70**, 10 (1987), 256.

[6] Park S.E., Shrout T.R.: Ultrahigh strain and piezoelectric behavior in relaxor based ferroelectric single crystals. *Journal of Applied Physics* **82** (1997), 1804.

[7] Luo H., Xu G., Wang P. and Yin Z.: Growth and characterization of relaxor ferroelectric PMNT single crystals. *Ferroelectrics* **231** (1999), 97.

[8] Park S.E. and Shrout T.R.: Characteristics of relaxor-based piezoelectric single crystals for ultrasonic transducers. *IEEE Transactions on Ultrasonics, Ferroelectrics, and Frequency Control* **44** (1997), 1140.

[9] Peng J., Chen J. and Luo H: Shear-mode piezoelectric properties of $0.69Pb(Mg_{1/3}Nb_{2/3})O_3$-$0.31PbTiO_3$ single crystals. *Solid State Community* **130** (2004), 53.

[10] Ujiie R, Uchino K.: *Proceeding IEEE Ultrasonic Symposium* 1991; 725.

[11] Viehland D.: Symmetry-adaptive ferroelectric mesostates in oriented $Pb(BI_{1/3}BII_{2/3})O_3$-$PbTiO_3$ crystals. *Journal of Applied Physics* **88** (2000), 4794.

[12] Kuwata J., Uchino K. and Nomura S.: *Ferroelectrics* **37** (1981), 579.

[13] Ren W., Liu S-F. and Mukherjee B.K.: Piezoelectric properties and phase transitions of [001]-oriented $Pb(Zn_{1/3}Nb_{2/3})O_3$-$PbTiO_3$ single crystals. *Appl. Phys. Lett.* **80** (2002), 3174.

[14] Liu S., Park S.E., Shrout T.R. and Cross L.E.: *Journal of Applied Physics* **85** (1999), 2910.

[15] Lu Y, Jeong D-Y, Cheng Z-Y, Zhang QM.: *The Tenth US–Japan Seminar on dielectric and piezoelectric ceramics* (2001), 257.

[16] Forrester J. S., Kisi E.H. and Knight K.S.: Phase transitions in PZN-4.5%PT in the range 4.2–450 K. *Physica B: Condensed Matter* **385-386** (2006), 160.

[17] Rajana K.K., Shanthia M., Changa W.S., Jinb J. and Lima L.C.: Dielectric and piezoelectric properties of [0 0 1] and [0 1 1]-poled relaxor ferroelectric PZN-PT and PMN-PT single crystals. *Sensors and Actuators A: Physical* **133** (2007), 110.

[18] Jue Penga, Haosu Luob, Tianhou Heb, Haiqing Xub and Di Lin.: Elastic, dielectric, and piezoelectric characterization of $0.70Pb(Mg_{1/3}Nb_{2/3})O_3$-$0.30PbTiO_3$ single crystals. *Materials Letters* **59** (2005) 640.

[19] Shen M., Yao D. and Cao W.: Study of electric-field-induced phase transitions in [111] oriented $0.955Pb(Zn_{1/3}Nb_{2/3})O_3$-$0.045PbTiO_3$ single crystals. *Materials Letters* **59** (2005), 3276.

[20] Zhang R., Jiang B., Jiang W. and Cao W.: Complete set of properties of $0.92Pb(Zn_{1/3}Nb_{2/3})O_3$-$0.08PbTiO_3$ single crystal with engineered domains. *Materials Letters* **57** (2003), 1305.

[21] Yin J.; Jiang B.; Cao W.: Elastic, piezoelectric, and dielectric properties of $0.955Pb(Zn_{1/3}Nb_{2/3})O_3$-$0.45PbTiO_3$ single crystal with designed multidomains. *IEEE Transactions on Ultrasonics, Ferroelectrics and Frequency Control,* **47** (2000), 285.

[22] Yin J., Cao, W.: *Journal of Applied Physics Letters* **80**, (2002), 1043.

[23] Yin J., Cao W.: Polarization reversal study using ultrasound. *Applied Physics Letters* **79**, 27 (2001), 4556.

[24] Jiang W., Zhang R., Jiang B., Cao W.: Characterization of piezoelectric materials with large piezoelectric and electromechanical coupling coefficients. *Ultrasonics* **41**, Issue 2 (2003), 55.

[25] Hwa L. G., Chao W. C.: *Material Chemistry and Phys*ics **94**, 37 (2005).

[26] Su J. R., Zhu C.F., Wang M. and Zhu Z. G.: Studies of the ultrasonic properties of triglycine sulfate (tgs) single crystal**.** *Materials Research Bulletin* **34**, Issues 12-13 (1999), 1885.

[27] Hwa L. G., Chao W. C., Szu S.P.: Pressure and temperature dependence of elastic properties of lanthanum gallogermanate glasses**.** *Materials Research Bulletin* **37***,* Issue 7 (2002), 1293.

[28] Kumagai T., Nakanishi Y., Sugawara H., Sato H. and Yoshizawa M: Elastic properties of Re-Ru_4Sb_{12} (Re; La, Pr), *Physica B: Condensed Matter* **329-333**, Part 2 (2003), 471.

[29] Royer D, Dieulesaint E.: Elastic Waves in Solids I, II. Springer-Verlag Berlin, Heidelberg, New York, 2000.

[30] Obraz J.: Zkoušení materiálu ultrazvukem. SNTL, Praha, 1989.

[31] Ryzhenko V, Burianova L, Hana P.: Influence of electric field on the ultrasound velocity in PZT ceramics. *Journal of Electroceramics* **20** (2008), 35.

[32] Hana P., Burianova L., Furman E., Zhang S., Shrout T. R., Ryzhenko V., Burry P.: Elastic stiffness constants of PZN-4.5%PT single crystal influenced by dc bias electric field applied at various directions to prototypic crystal symmetry. *Ferroelectrics* **319** (2005), 371.

[33] Hana P, Bury P, Burianova L, Zhang S. J., Shrout T. R., Ryzhenko V.: Temperature and electric field dependence of ultrasonic wave propagation and attenuation in PZN-PT single crystal in vicinity of a phase transition. *Journal of Electroceramics* **20** (2008), 27.

[34] Cheeke J.D.N.: Fundamentals and Applications of Ultrasonic Waves, CRC Press London, New York, Washington D.C., 2002.